

A. 1-68-89-II
July 20, 1968

TM-151
2610.2
2630.2

FAKE STUDIES OF SOME STRONG AND WEAK INTERACTIONS
IN THE 12-FT AND 25-FT BUBBLE CHAMBERS

PART II. STRONG INTERACTIONS

M. Derrick
Argonne National Laboratory

T. O'Halloran
University of Illinois

and

R. Kraemer
Carnegie-Mellon University

Introduction

The error formulae and the parameters of the chambers are given in Part I of this report which deals with neutrino interactions. The experiments with hadron beams represent a much larger class of possibilities which could not be properly explored because of the limitations of time. The work was concentrated on 4c types since it is obvious that the 4c events will be much more difficult to handle even using neutron recoils or γ -ray conversions in the chamber. We decided to try events of different characteristics including a class dominated by a single fast forward-going track, and so chose elastic scattering. It is of course unlikely that a bubble chamber would be used to study such reactions, but the technique is used extensively now for similar reactions such as $m + B \rightarrow m^* + B$. As a contrast, we also generated a reaction involving six secondary charged particles which is perhaps a more typical final state at high energies.

Strong-Interaction Events Generated

The different types of event that were generated were specifically:

1. $K^- p \rightarrow K^- p$ with a c.m. angular distribution $d\sigma/dt \propto e^{6t}$
2. $\bar{p}p \rightarrow 3\pi^+ 3\pi^-$ with the pions distributed according to phase space in the c.m.
3. $K^- p \rightarrow K^{*-} p$ with a c.m. angular distribution $d\sigma/dt \propto e^{6t}$
 \downarrow
 $K^0 \pi^-$
 \downarrow
 $\pi^+ \pi^-$

Two of the pions in reaction 2 were constrained to be in a resonance of mass 1 GeV and width 10 MeV with zero spin. The first two reactions were generated at 50 GeV/c, 100 GeV/c, and 200 GeV/c incident-beam momenta, whereas reaction 3 was only studied at 100 GeV/c. In all cases the beam-momentum spread was taken to be $\Delta p/p = \pm 0.1\%$.

The three examples chosen give final states with 2, 6 and 4 prongs. The $K^- p$ elastic events have the characteristic of a single very high momentum forward track which favors the 25-ft chamber since the momentum precision is measurement limited and long tracks are needed.

The 6-prong $\bar{p}p$ annihilations simulate a class of events which could be produced by a multiperipheral process. Such events will probably become more important as the energy increases. Even at present energies, where two-body final states are quite strong, most of the inelastic cross section seems to represent multibody final states.

The same canonical four sets of chamber parameters were used as in the ν study, that is:

(i) 12-ft chamber	20 kG	250 μ setting error
(ii) 12-ft chamber	40 kG	250 μ setting error
(iii) 25-ft chamber	40 kG	250 μ setting error
(iv) 25-ft chamber	40 kG	500 μ setting error

K^-p ELASTIC SCATTERING

Results from FAKE

In Table I we show the results for a typical event at 50 GeV/c in the four chambers. About 60% of the protons stop in the hydrogen (12 ft, 40 kG) which is a great advantage of these big chambers. Figures 1-3 show the momentum precision on the secondary kaon track as a function of track length for 50, 100, and 200 GeV. In all cases the scattered kaon has nearly the same momentum as the beam. The long tracks are multiple-scattering limited, and it is clear that the 25-ft chamber has tracks in this regime even up to 200 GeV. Comparing cases (ii) and (iv) at 50 GeV/c, the ultimate precision is about the same provided one allows 3 m of secondary track in the 12-ft chamber. At 200 GeV/c, however, the 12-ft chamber is clearly getting too small for this kind of event, and even the 25 ft is being pushed to its limits.

The accuracy of momentum measurement on this track obviously dominates the situation. The beam-momentum spread of 0.1% is negligible in comparison. For this particular type of event then a tighter beam momentum spread will not help the kinematics.

The transverse momentum unbalance (ΔP_T) is shown in Figs. 4

Table I. FAKE Results for a Typical Event $K^- p \rightarrow K^- p$
At 50 GeV/c in the Four-Chamber Parameter Combinations.

		X	Y	Z	DX	DY	DZ			
Vertex coordinates		-141.22	6.64	-99.95	0.025	0.025	0.025	Chamber (a) 12 ft, 40 kG, 250 μ		
		Millirad			Errors			Cm	Micron	
Track	Charge	MeV/c P	Dip	Phi	ΔP	$\Delta \lambda$	$\Delta \phi$	Length	+ -	Sagitta
1	-	139162	-0	3141	176661	1	3	-51.03	0.05	140 interacts
2	-	50235	-2	6282	557	0	0	333.33	0.05	-16588
3	+	376	254	1363	8	14	20	32.21	0.10	20013 stops

		X	Y	Z	DX	DY	DZ			
Vertex coordinates		-141.22	6.80	-99.95	0.025	0.025	0.035	Chamber (b) 12 ft, 40 kG, 250 μ		
1	-	43545	-0	3147	24675	1	3	-51.03	0.05	531 interacts
2	-	50070	-2	5	287	0	0	332.87	0.05	-33194
3	+	378	254	1369	4	14	20	32.21	0.10	39850 stops

		X	Y	Z	DX	DY	DZ			
Vertex coordinates		-315.93	7.33	-149.92	0.025	0.025	0.052	Chamber (c) 25 ft, 40 kG, 500 μ		
1	-	56598	-0	3158	5400	1	2	-83.98	0.05	1869 interacts
2	-	49862	-2	13	91	0	0	712.75	0.05	-152828
3	+	378	256	1377	4	14	20	32.20	0.10	39814 stops

		X	Y	Z	DX	DY	DZ			
Vertex coordinates		-315.89	7.29	-149.84	0.050	0.050	0.104	Chamber (d) 25 ft, 40 kG, 500 μ		
1	-	65450	-1	3154	14434	2	4	-83.98	0.10	1616 interacts
2	-	49931	-2	13	136	0	0	712.78	0.10	-152628
3	+	380	261	1370	5	15	21	32.21	0.20	39599 stops

and 5 for the 50 GeV/c and 200 GeV/c cases. This variable is dominated by the recoil proton so the change with beam momentum is not strong. All cases are comparable with ΔP_T approximately 50 MeV/c for 50 GeV and 100 MeV/c for 200 GeV. The beam momentum spread of 0.1% $\Delta p/p$ together with the much larger $\Delta p/p$ on the secondary track (Figs. 1-3) give a longitudinal momentum unbalance (ΔP_L) that increases faster than the momentum. The ΔP_L comes from the secondary-kaon track and is typically 250 MeV/c for 50 GeV and 1400 MeV/c for 200 GeV for case (iv) and twice as large for case (ii) for events in the fiducial region which we take to be the upstream half of the chamber.

The total c.m. energy for events occurring in the fiducial volume is shown in Figs. 6-8 for the three beam momenta. On each figure a scale of 280 MeV ($\pm 1 \pi^0$ mass) is shown for comparison. At the lowest momentum the width of the distributions is quite tight with a full width in the range 50 to 100 MeV with chambers (ii) and (iv) comparable, whereas at 200 GeV the resolution is becoming marginal and only the 25-ft chamber with 250 μ setting error has nearly enough accuracy. At 100 GeV/c case (iv) still gives a tight distribution, whereas the 12-ft chamber with 20 kG is clearly inadequate.

Results of Fitting

The results of fitting, about 50 such events for each momentum and chamber combination are summarized in Table II. The events listed in the Table are just those with primary vertex in the upstream half of the chamber.

Table II. Results of Fitting a Small Number of Events for each Combination.

Beam Momentum GeV/c	Chamber			Total Events	Unique Fits	2 - Fold	3 - Fold
	size feet	B Field kG	ϵ			Ambiguous Fits	Ambiguous Fits
50	12	20	250	23	14	8	1
50	12	40	250	23	15	8	0
50	25	40	250	28	24	3	1
50	25	40	500	28	24	4	0
100	12	20	250	27	10	13	4
100	12	40	250	27	13	11	3
100	25	40	250	29	20	8	1
100	25	40	500	29	18	9	2

All events were ambiguous with πp or pp elastic scattering but this was neglected. Assuming the incident beam to be pure kaons, then the hypotheses tried were

- (i) $K^- p \rightarrow K^- p$ generated
- (ii) $K^- p \rightarrow K^- p \pi^0$
- (iii) $K^- p \rightarrow \pi^- p \bar{K}^0$ with the \bar{K}^0 missing
- (iv) $K^- p \rightarrow K^- \pi^+ n$.

The column labeled 2-fold ambiguous means that one of the hypotheses, (ii), (iii), or (iv), gave a fit (with χ^2 probability $> 1\%$) in addition to the elastic fit. The 3-fold ambiguous events gave fits to two of the three inelastic hypotheses in addition to the elastic fit.

At 200 GeV/c there was evidence that the fitting program had some convergence problems, so the results are unreliable and are not given.

The results are encouraging and support the conclusions one would draw from the FAKE data presented earlier. The fraction of ambiguities is quite similar to those obtained today in smaller

chambers with lower-momentum beams. The 25-ft chamber is clearly superior to the 12 ft because of the extra track length available and can be used for this kind of experiment to somewhere beyond 100 GeV but less than 200 GeV, whereas the 12-ft chamber probably cuts out below 100 GeV/c.

$\bar{p}p$ ANNIHILATIONS TO SIX-CHARGED PIONS

Results from FAKE

The results for this final state are quite different from the elastic scattering. The momentum spectrum of the pions for 100-GeV incident antiprotons is shown in Fig. 9. The average momentum is about 13 GeV/c as expected ($100/6$) with very few tracks having momenta greater than 50 GeV/c. The tracks are peaked forward at all energies, in general coming out within a cone of approximately 18° half angle at 100 GeV/c (see Fig. 10).

The relatively low momentum of the secondary tracks combined with a 40 kG field spreads out the pions so they leave the chambers over a large fraction of the downstream wall, as can be seen in Fig. 11 which shows the end points of all the tracks, including the beam antiproton for the 12 ft and 25-ft chambers with 40 kG and 100-GeV incident beam momentum. The beam is clearly delineated. Points not on the chamber wall represent tracks that gave a secondary interaction in the hydrogen. Any neutral pions produced in the reaction would fall inside the 18° cone and the γ rays from the π^0 decays will only widen this distribution by a few degrees. It is clear then that any region in the downstream part of

the chamber for γ -ray conversion will also intersect a large fraction of the secondary-pion tracks. These secondary pions will give many interactions in the neon or plate region and lead to great confusion in scanning for γ rays from the primary vertex.

Table III gives the FAKE printout for a typical event at 100 GeV/c in the four chamber combinations. The beam momentum is unmeasured in all cases since the beam track is very short. The third secondary track interacts and, for the 25-ft chamber, so also does the first secondary track. Chambers (ii) and (iv) have comparable errors.

The momentum precision on the secondary tracks for the four chambers at the three energies is shown in Figs. 12-14. The values now cover a wide band, since the annihilation pions cover a wide momentum spectrum unlike the scattered kaons in the previous reaction. For the $\bar{p}p$ annihilation the 12-ft chamber with 40 kG has a region with tracks which are scattering limited even as high as 100 GeV/c, whereas at 200 GeV/c only the 25-ft chamber is long enough. At 50 GeV the chambers are comparable in accuracy for the longest tracks.

At 100 GeV/c the long tracks give $\Delta p/p$ in the range 0.3% to 0.6% for cases (ii) 12 ft, 40 kG, 250 μ and (iv) 25 ft, 40 kG, 500 μ . Since the mean momentum of the pions is 6 times lower than the beam, a beam-momentum spread of 0.05% to 0.1% is required to match the error per track. Since there are six secondary particles, a beam momentum spread of 0.1% is adequate.

The last two pions of the six were made in a resonance of mass

Table III. FAKE Results for a Typical Event $\bar{p}p \rightarrow 3\pi^+ 3\pi^-$
At 100 GeV/c in the Four-Chamber Parameter Combinations.

			X	Y	Z	DX	DY	DZ			
Vertex coordinates			-181.15	-1.76	-99.98	0.025	0.025	0.035	Chamber (a) 12 ft, 20 kG, 250μ		
			Millirad								
Track	Charge	MeV/c	Errors					Cm Length	+-	Micron Sagitta	
		P	Dip	Phi	ΔP	Δλ	Δφ				
1	-	10022	1	3148	18779	6	13	-111.27	0.05	95	interacts beam
2	+	31998	91	111	213	0	0	374.48	0.07	32735	
3	+	2164	303	416	9	2	3	337.06	0.11	375675	
4	-	11647	-5	6262	120	0	1	178.43	0.05	-20500	interacts
5	-	30960	-27	6197	202	0	0	373.16	0.06	-33721	
6	+	18608	-129	6216	94	0	0	373.66	0.08	55809	
7	-	5643	-46	6256	22	1	1	371.99	0.06	-183706	

			X	Y	Z	DX	DY	DZ			
Vertex coordinates			-181.15	-1.75	-99.98	0.025	0.025	0.035	Chamber (b) 12 ft, 40 kG, 250 μ		
1	-	18224	1	3149	31038	6	13	-11.27	0.05	105	interacts beam
2	+	32032	91	111	107	0	0	375.30	0.07	65687	
3	+	2167	303	416	5	2	3	337.06	0.11	750375	
4	-	11689	-5	6263	60	0	1	178.43	0.05	-40853	interacts
5	-	30921	-27	6197	101	0	0	373.95	0.06	-67814	
6	+	18616	-129	6217	47	0	0	370.88	0.08	109920	
7	-	5667	-46	6256	11	1	1	362.03	0.06	-346560	

			X	Y	Z	DX	DY	DZ			
Vertex coordinates			-381.78	-1.74	-99.96	0.025	0.025	0.062	Chamber (c) 25 ft, 40 kG, 250 μ		
1	-	36942	1	3147	48655	8	8	-18.25	0.05	135	interacts beam
2	+	32053	91	112	72	0	0	503.07	0.07	117943	interacts
3	+	2167	303	417	5	2	3	337.06	0.11	750365	
4	-	11689	-5	6263	60	1	1	178.43	0.05	-40854	interacts
5	-	30875	-27	6198	45	0	0	783.65	0.06	-298242	
6	+	18606	-129	6217	26	0	0	759.05	0.08	460640	
7	-	5673	-45	6258	8	1	1	673.02	0.06	-1196285	

Table III. (Continued)

Vertex coordinates X Y Z DX DY DZ
 -381.76 -1.69 -99.91 0.025 0.025 0.025

Chamber (d) 25 ft, 40 kG, 500 μ

Millirad

Errors

Cm
Length

+-

Micron
Sagitta

Track	Charge	MeV/c P	Dip	Phi	ΔP	$\Delta \lambda$	$\Delta \phi$				
1	-	22675	3	3151	36436	16	17	-18.31	0.10	222	interacts beam
2	+	32022	91	112	110	5	1	505.12	0.14	118078	interacts
3	+	2167	303	417	5	2	3	336.99	0.21	750045	
4	-	11647	-4	6264	106	2	2	178.36	0.10	-40969	interacts
5	-	30891	-26	6198	55	0	0	783.65	0.11	-298087	
6	+	18612	-128	6217	29	0	1	759.12	0.15	460597	
7	-	5673	-45	6257	8	1	1	673.10	0.12	-1196612	

-10-

TM-454
 2610.2
 2630.2

1 GeV and width 10 MeV. The effective mass plot of these two particles for the 50 GeV and 200-GeV beam momenta is shown in Figs. 15 and 16. There is very little to choose between the different chambers in this variable and the variation with beam momentum is not strong, probably because angle errors are very important for this low a mass resonance (see Derrick and Kraemer's report on optimum magnetic fields). In all cases the width is to 40 MeV, which means resonance-mass resolution will not be a serious problem for most experiments.

The total c.m. energy as measured from the secondary pions only is shown in Figs. 17-19 for events occurring upstream in the chambers. At 50 GeV/c the distributions are less than 100 MeV wide and this is maintained for the three chamber examples with 40-kG magnetic fields at 100 GeV. At 200-GeV incident momentum the widths have approximately doubled and the discrimination against an additional π^0 is becoming marginal, except for case (iii) 25 ft, 250 μ . The events not in the central peak come from those with pion tracks shortened by secondary interactions.

Secondary Interactions

For 100 GeV the six pion annihilations were generated with two values of the πp cross section of 25 mb and 50 mb which simulate a hydrogen and deuterium filling of the chamber. All the remaining events discussed in this report were generated with a secondary cross section of 25 mb. The number of events having 1 to 6 secondary tracks interacting is shown in Fig. 20. For a hydrogen filling about half the

secondary tracks interact before leaving the chamber for the case of the 25 ft, whereas for deuterium two-thirds interact. This has two bad effects. First, it clutters up the picture with unwanted tracks, particularly in the far downstream end, and, second, it restricts the possible track length so the momentum accuracy suffers. The situation clearly gets worse as the multiplicity increases, and it will probably be necessary to operate the chambers with only one or two beam tracks. A chamber as large as 25 ft may be too big for this kind of experiment.

The effect on the kinematics can roughly be seen by looking at the total c.m. energy for the events. For the worst case (25-ft chamber, 50 mb) the events having one or two secondary tracks interacting all have the c.m. energy within 100 MeV of the central value whereas only about half the events with more than two tracks interacting fall within that limit. This then reduces the counting rate by about a factor of two. The main problem will be that all events will need measuring since the rejections must be based on kinematic variables rather than on scanning criteria. It is clearly not possible to only accept events in which no secondary track interacts. This points up a major weakness of the bubble-chamber technique if one extrapolates experiments done today to higher energies.

The individual cross sections are decreasing rapidly as the beam energy increases. The larger chambers necessary for measurement accuracy will not increase the event rate as most of the chamber is only needed for measuring the secondary tracks and the increase in

fiducial length will be compensated by the fewer beam tracks that can be used. The secondary interactions further reduce the counting rate. Long runs of the chambers will then be necessary to accumulate enough events.

Results of Fitting

All the events were fit using GRIND. For almost all cases, a fit could be obtained where some $\pi^+\pi^-$ pair was replaced by a K^+K^- pair, so no chamber had sufficient precision to discriminate against this possibility. At lower energies bubble density is used to help this separation, but this is no use at the energies considered here. A small fraction of the events with K pairs could be identified when both kaons interact in the chamber.

The remaining hypotheses were 4c (6 charged pions) and 1c (6 charged pions plus 1 π^0). The fraction of events that gave only a 4c fit are listed in Table IV for events with the primary vertex occurring upstream in the chamber. Additional information could be used to improve these fractions, but even with the numbers given, it seems that this type of event can usefully be studied up to about 200 GeV. Up to 100 GeV the 12-ft chamber with 40 kG and 250 μ is as good as the 25-ft chamber with 40 kG and 500 μ .

K^* PRODUCTION IN K^-p COLLISIONS

This reaction has been calculated only at 100 GeV/c. The total c.m. energy for the four chambers for events occurring anywhere in

Table IV. $\bar{p}p \rightarrow 3\pi^+ 3\pi^-$.

Beam Momentum	Chamber Combination	% of Events Giving Unique Fits
50 GeV/c $\pm 0.1\%$	12 ft 20 kG 250 μ	68
	12 ft 40 kG 250 μ	88
	25 ft 40 kG 500 μ	88
	25 ft 40 kG 250 μ	90
100 GeV/c $\pm 0.1\%$	12 ft 20 kG 250 μ	50
	12 ft 40 kG 250 μ	65
	25 ft 40 kG 500 μ	66
	25 ft 40 kG 250 μ	76
200 GeV/c $\pm 0.1\%$	12 ft 20 kG 250 μ	31
	12 ft 40 kG 250 μ	40
	25 ft 40 kG 500 μ	50
	25 ft 40 kG 250 μ	50

the chamber, showed no advantage for any chamber. The width was approximately 200 MeV which is worse than the $\bar{p}p$ case at the same energy. The requirement of a visible K^0 decay preferentially populates the upstream region of the chamber since all the K^0 's go forward.

The transverse-momentum distributions with the K^0 ignored are the same for all chambers which says that the P_T unbalance resulting from ignoring the K^0 is larger than the uncertainty in P_T coming from the measuring and multiple-scattering error. The P_T distributions were quite similar with only the 25 ft, 40 kG, 250 μ being noticeably sharper. The mean uncertainty on P_T was approximately 150 MeV/c which is greater than for the $\bar{p}p$ case probably because the K^0 decay-pion tracks were short and not well determined.

The resolution on the K^0 mass was about 30 MeV except for case (iii) 25 ft, 40 kG, 250 μ , which had a width of about 20 MeV. Angle errors were important for these K^0 's as the tracks are short.

The results of fitting the events are summarized in Table V.

Table V. $K^- p \rightarrow K^{*-} p$ at $100 \text{ GeV}/c \pm 0.1\%$.

$$\rightarrow K^0 \pi^-$$

$$\rightarrow \pi^+ \pi^-$$

Chamber Combination	Total	Unique	Ambiguous		No 4c Fit
	Fits		4c best	1c best	
12 ft 20 kG 250 μ	40	18	13	8	1
12 ft 40 kG 250 μ	41	29	5	3	4
25 ft 40 kG 250 μ	37	30	3	4	0
25 ft 40 kG 500 μ	43	21	10	11	1

The ambiguous column is divided into two sections depending on the relative χ^2 probability of the 4c or 1c fit. The 4c hypothesis was that generated whereas the 1c hypothesis was the final state $\bar{K}^0 \pi^- \pi^0$. The 12-ft chamber with 40 kG (ii) is slightly better than the 25 ft with 500 μ setting error (iv) and equally as good as (iii).

Conclusions and Further Studies

This work supports the results of hand calculations and previous computer work in the conclusion that strong-interaction events can be kinematically reconstructed at high energies with the new chambers. The exact upper limit of beam momentum is not sharp but $100 \text{ GeV}/c$ seems to be a reasonable value.

For cases having a larger number of charged particles in the final state, a smaller, high-precision chamber is more favored, and for six charged particles the 12-ft chamber is substantially as good as the 25-ft up to $100 \text{ GeV}/c$. Further comparisons of this type should wait on the actual performance of the 7-ft and 12-ft chambers, although further

work on the effect of the setting error, ϵ , would be useful covering the range say from 100μ to $1,000\mu$. For low-multiplicity events the proposed 25-ft chamber is clearly better than the 12 ft.

If one considers the 12-ft chamber at NAL as a strong-interaction tool, then a field of 40 kG is essential.

An incident beam-momentum bite of $\pm 0.1\%$ is adequate, and smaller values would not add much to the accuracy. This should be specifically checked by generating and fitting some events with different momentum bites in the beam.

This work has shown that events with no missing neutrals do not often give a fit with an additional neutral particle. Since the way 4c events are separated in a bubble-chamber experiment is to ignore any 1c fit ambiguous with a 4c, it is obviously of the first importance to generate some 1c events and see if they give a 4c fit. This should include events in which one of the γ rays from a π^0 converted in the hydrogen as a special 2c category.

Acknowledgments

This work was made possible by the help of Denise Pavis at Argonne and Ward Schultz at the University of Colorado.

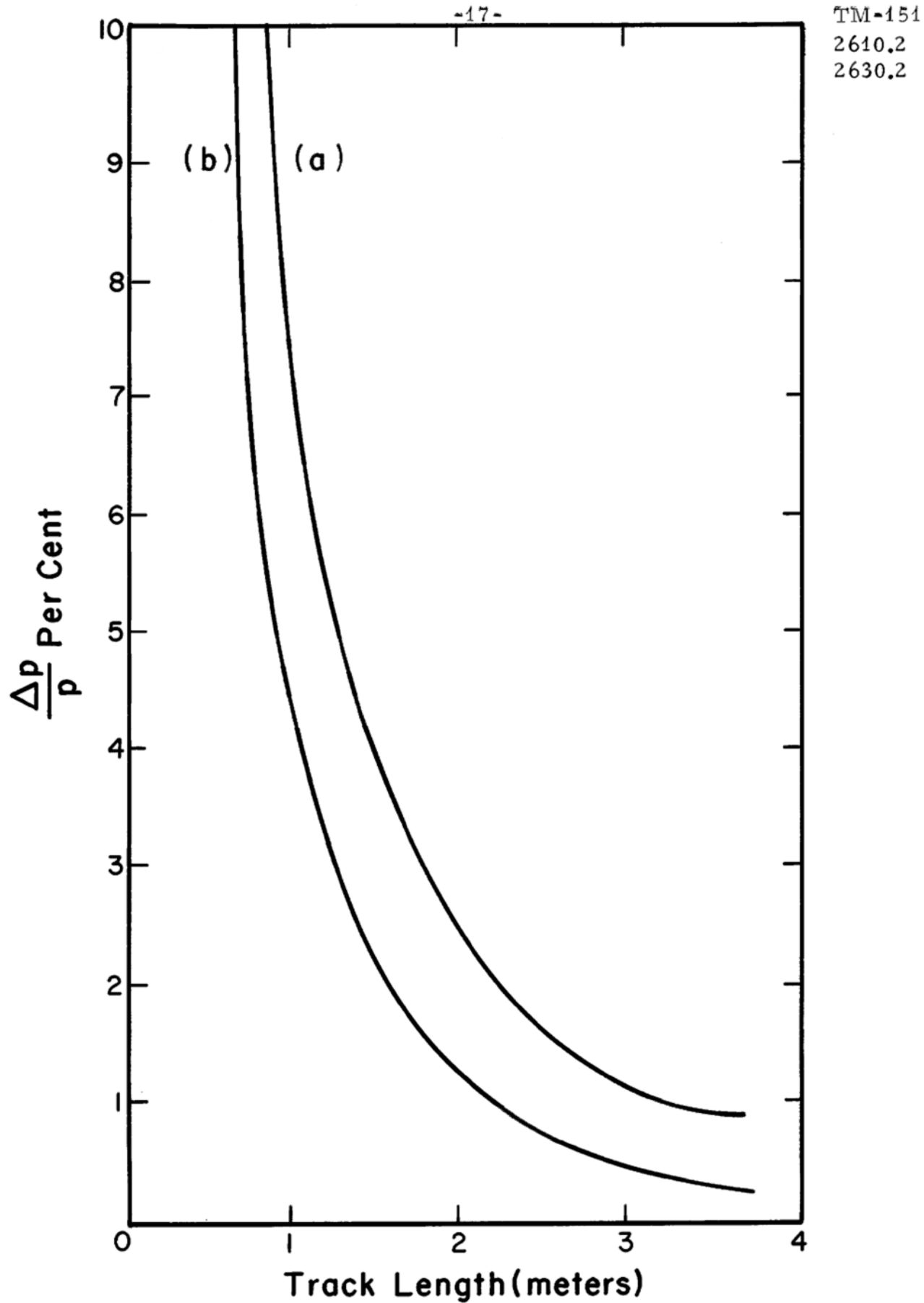


Fig. 1a. FAKE-generated curves of momentum error vs. track length, for the elastic scattering reaction $K^- + p \rightarrow K^- + p$ at 50 GeV/c; this plot is for the ANL 12-ft. chamber, with 20 kgauss magnetic field, setting $\epsilon = 250$ microns. 1b. Same as 1a, with magnetic field 40 kgauss.

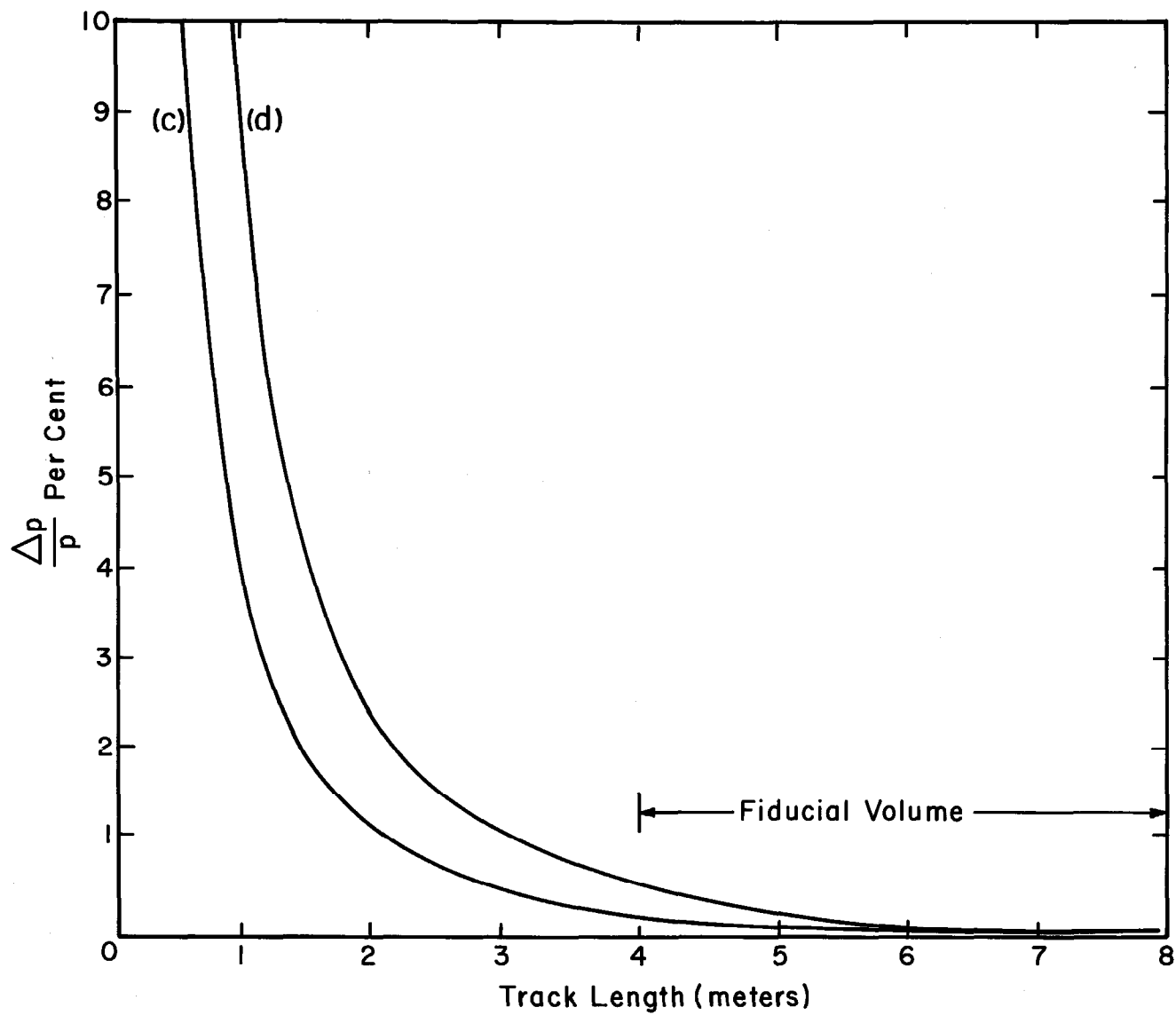


Fig. 1c. Same as 1a, with BNL 25-Ft. chamber, 40 kgauss field, setting error 250μ

Fig. 1d. Same as 1c, but setting error 500μ.

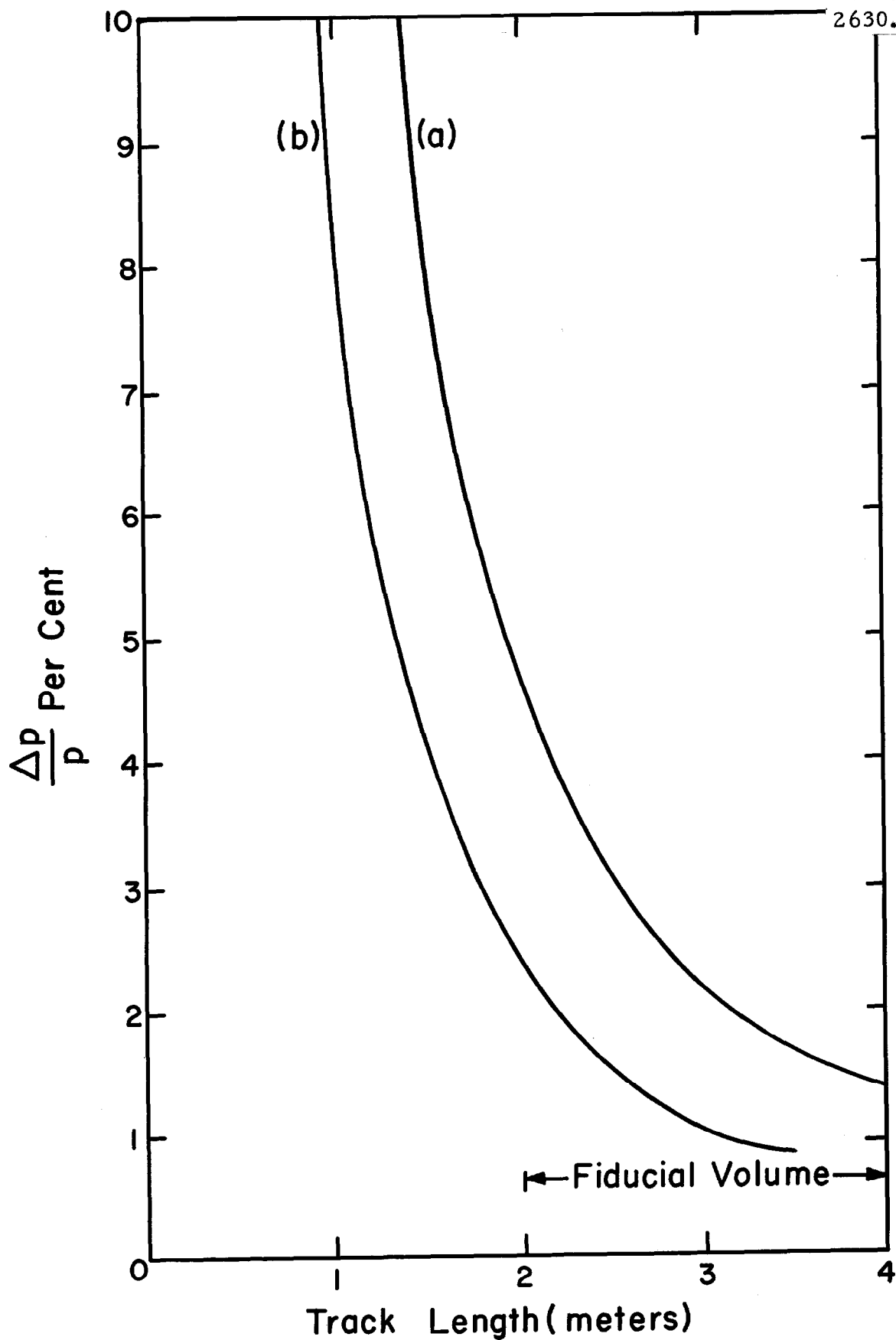


Fig. 2a. Same as 1a, except that K-p scattering is at 100 GeV/c.
2b. Same as 1b, except scattering is at 100 GeV/c.

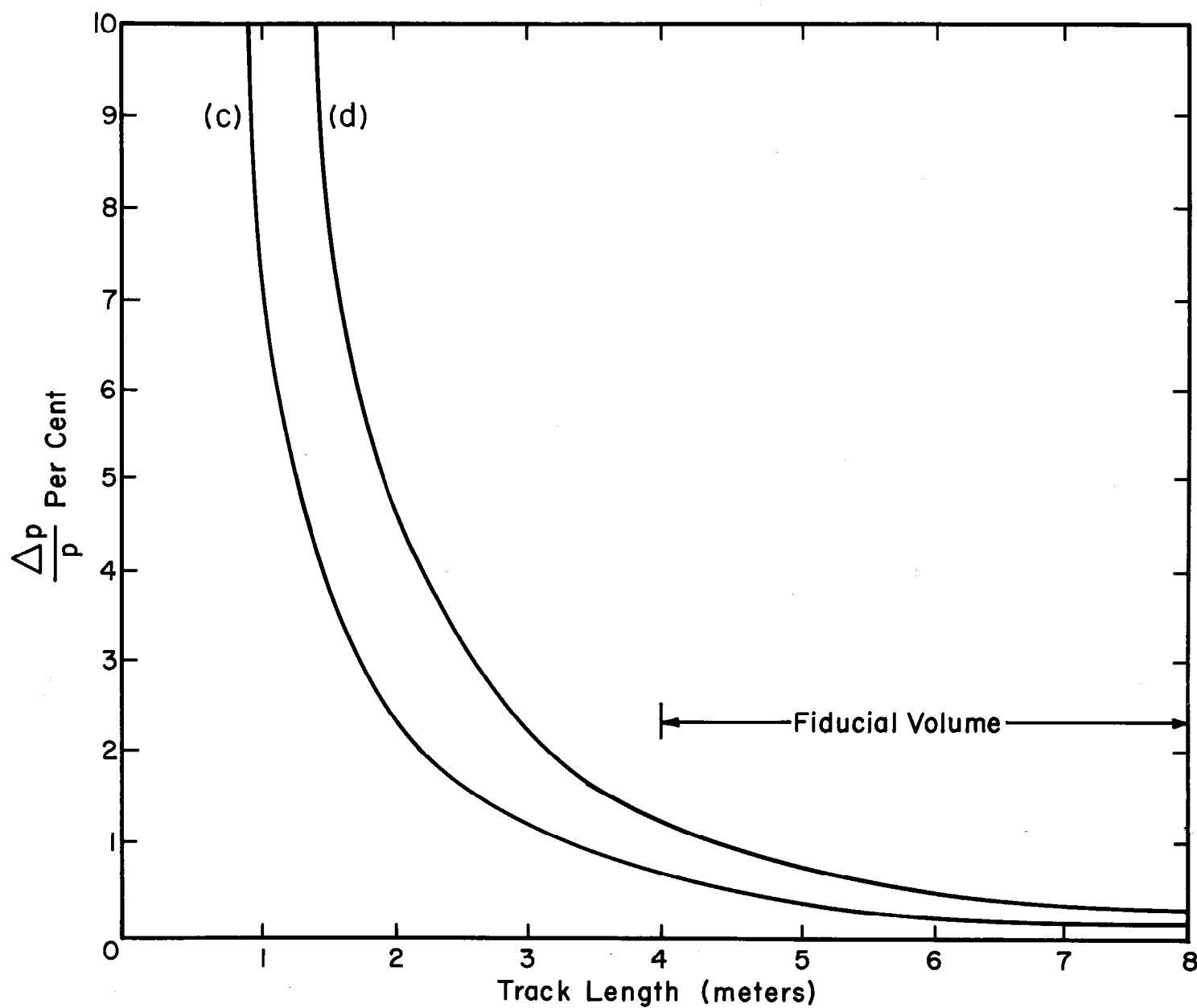


Fig. 2c. Same as 1c, for 100 GeV/c.

Fig. 2d. Same as 1d, for 100 GeV/c.

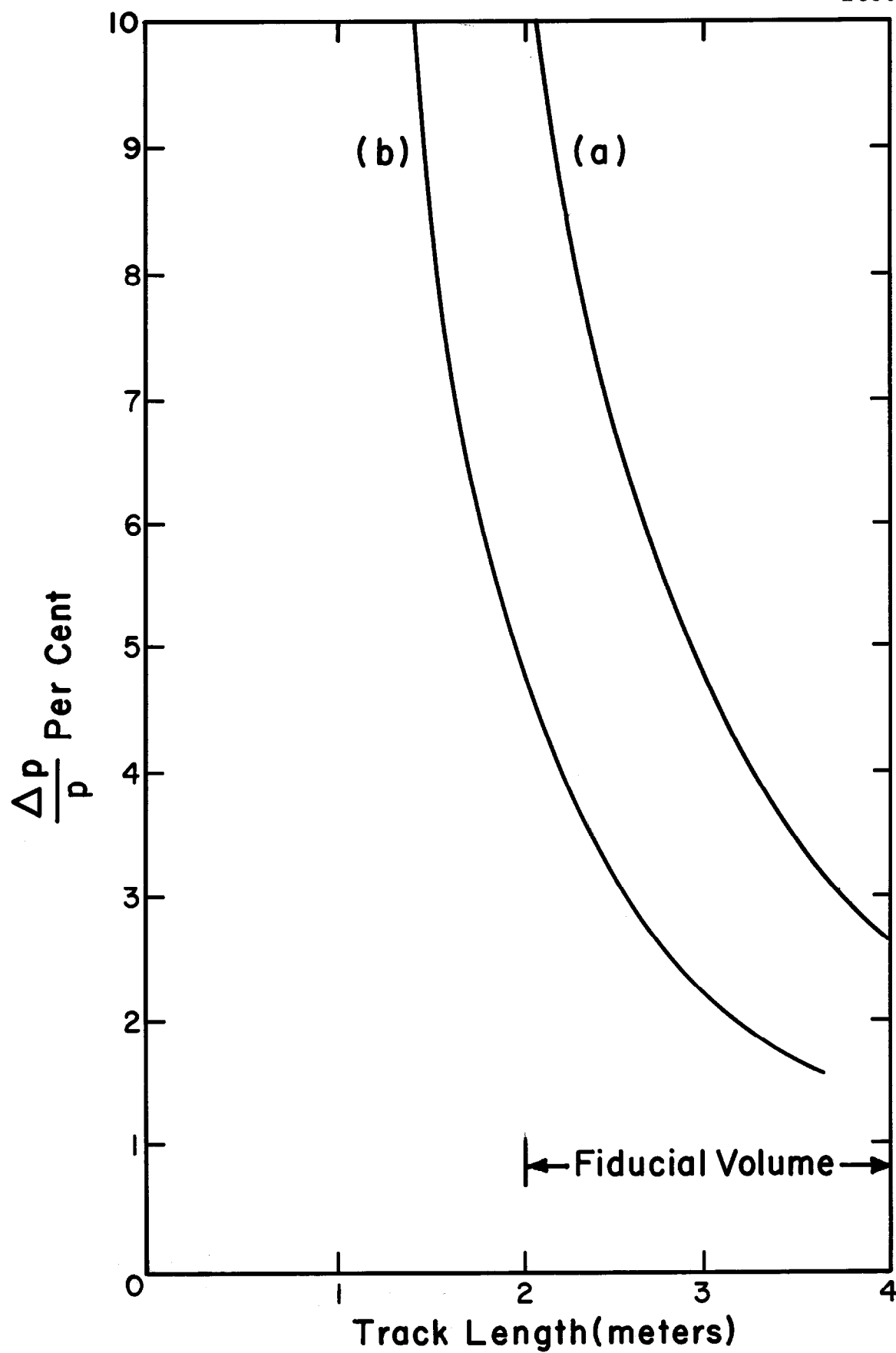


Fig. 3a. Same as 1a, for 200 GeV/c. 3b. Same as 1b, for 200 GeV/c.

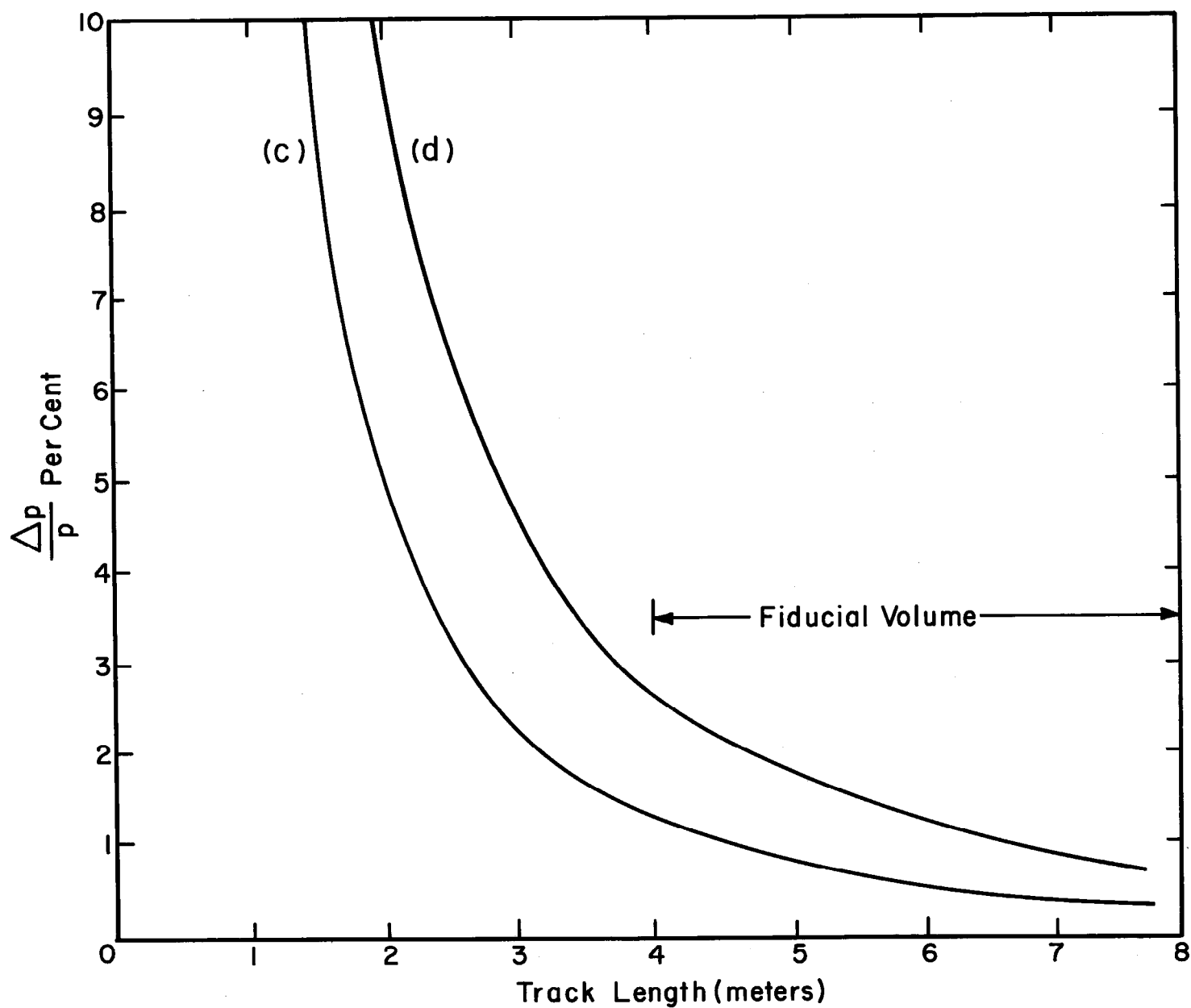


Fig. 3c. Same as 1c, for 200 Gev/c.

Fig. 3d. Same as 1d, for 200 Gev/c.

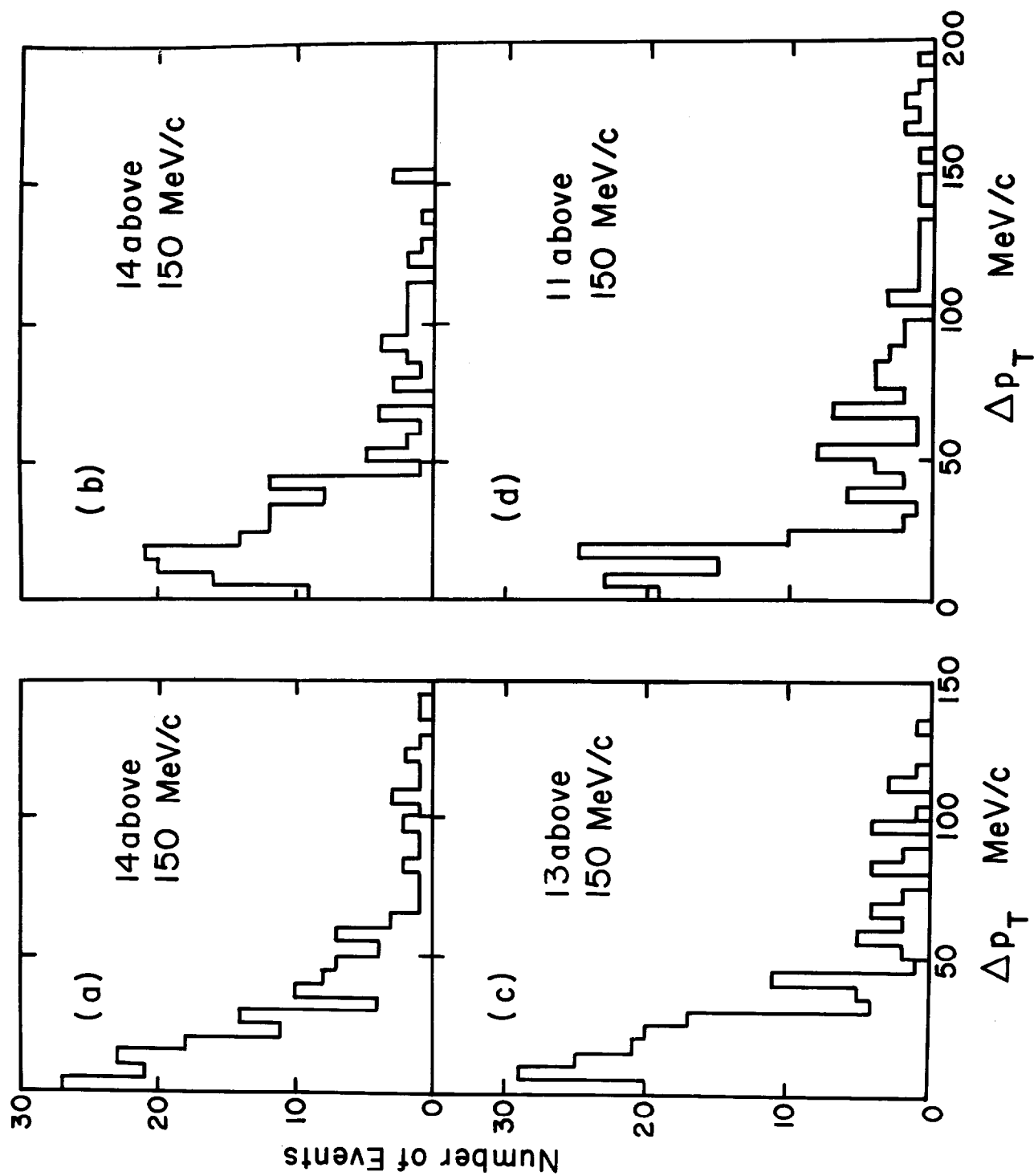


Fig. 4. Spectrum of transverse momentum unbalance for 200 events of K^-p elastic scattering at 50 GeV/c, showing events above 150 MeV/c as overflow. (a) 12-ft chamber, 20-kG field, $\epsilon = 250\mu$. (b) Same, with 40 kG. (c) 25-ft chamber, 40 kG, $\epsilon = 250\mu$. (d) Same, with $\epsilon = 500\mu$.

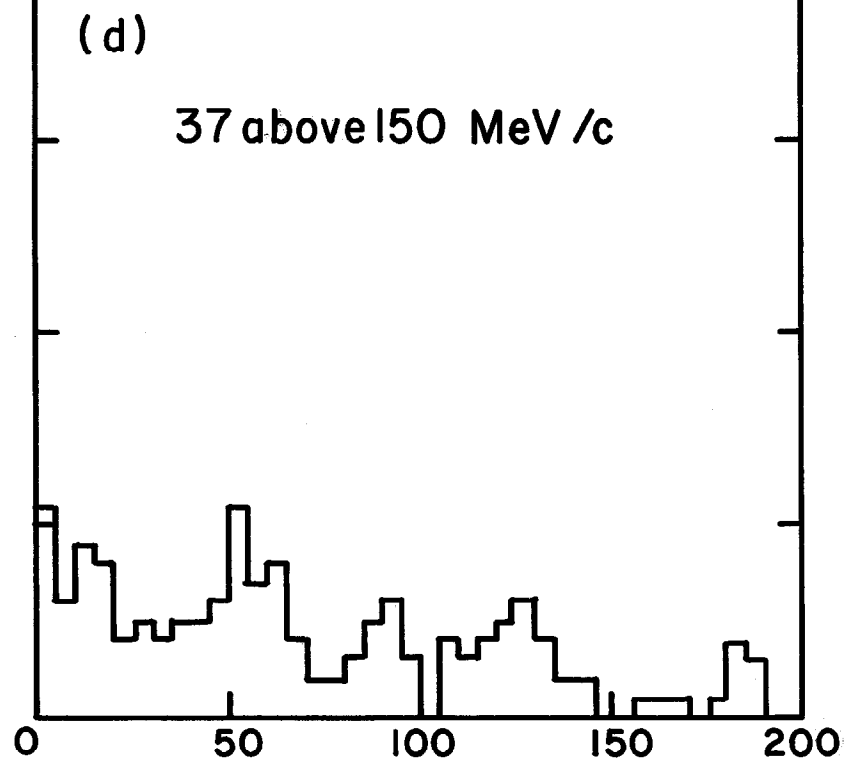
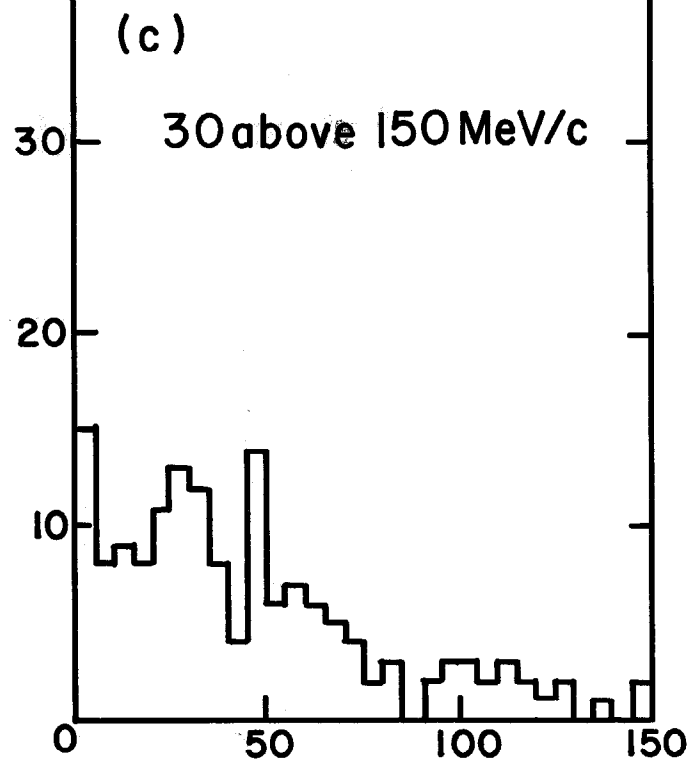
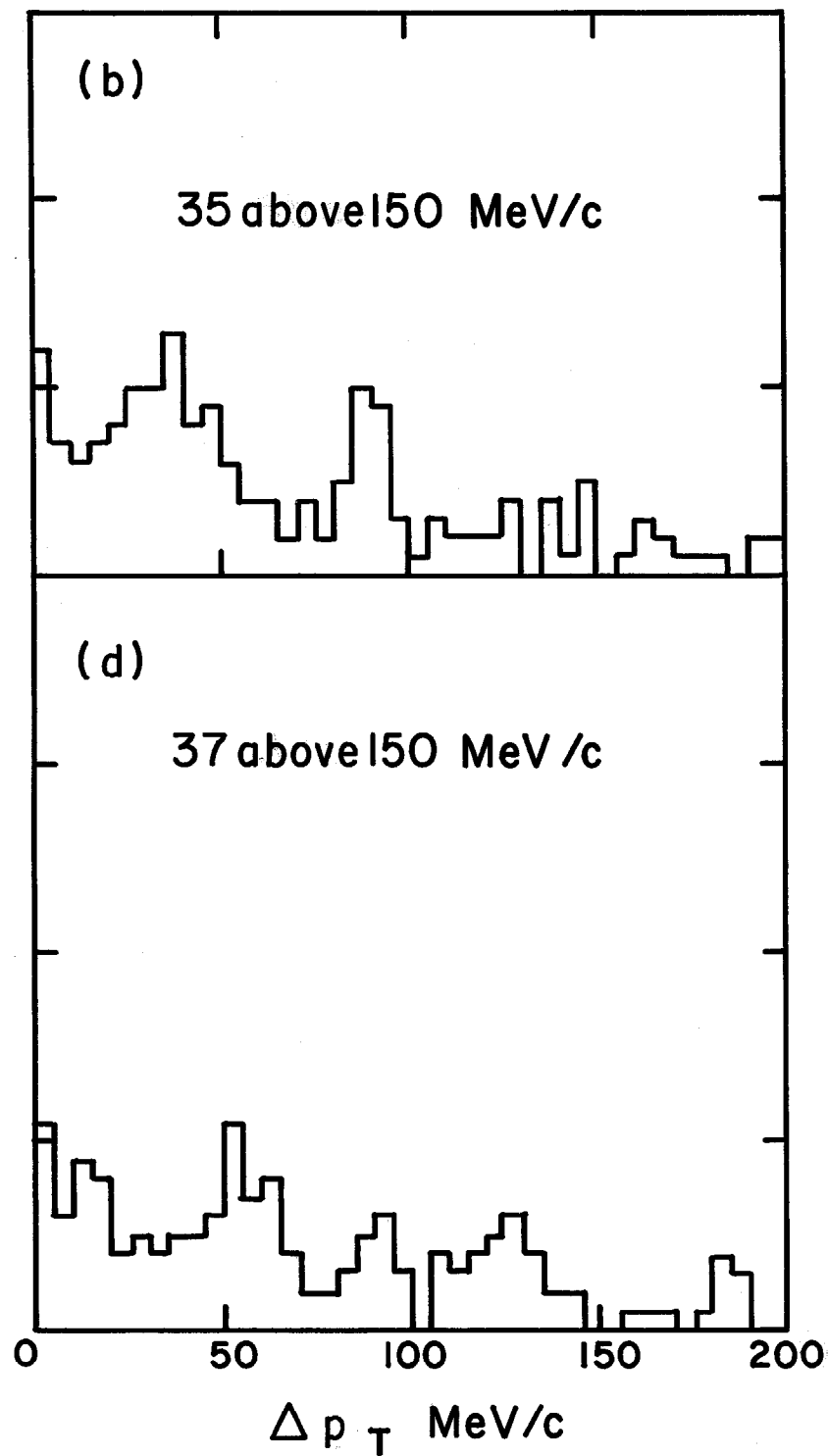
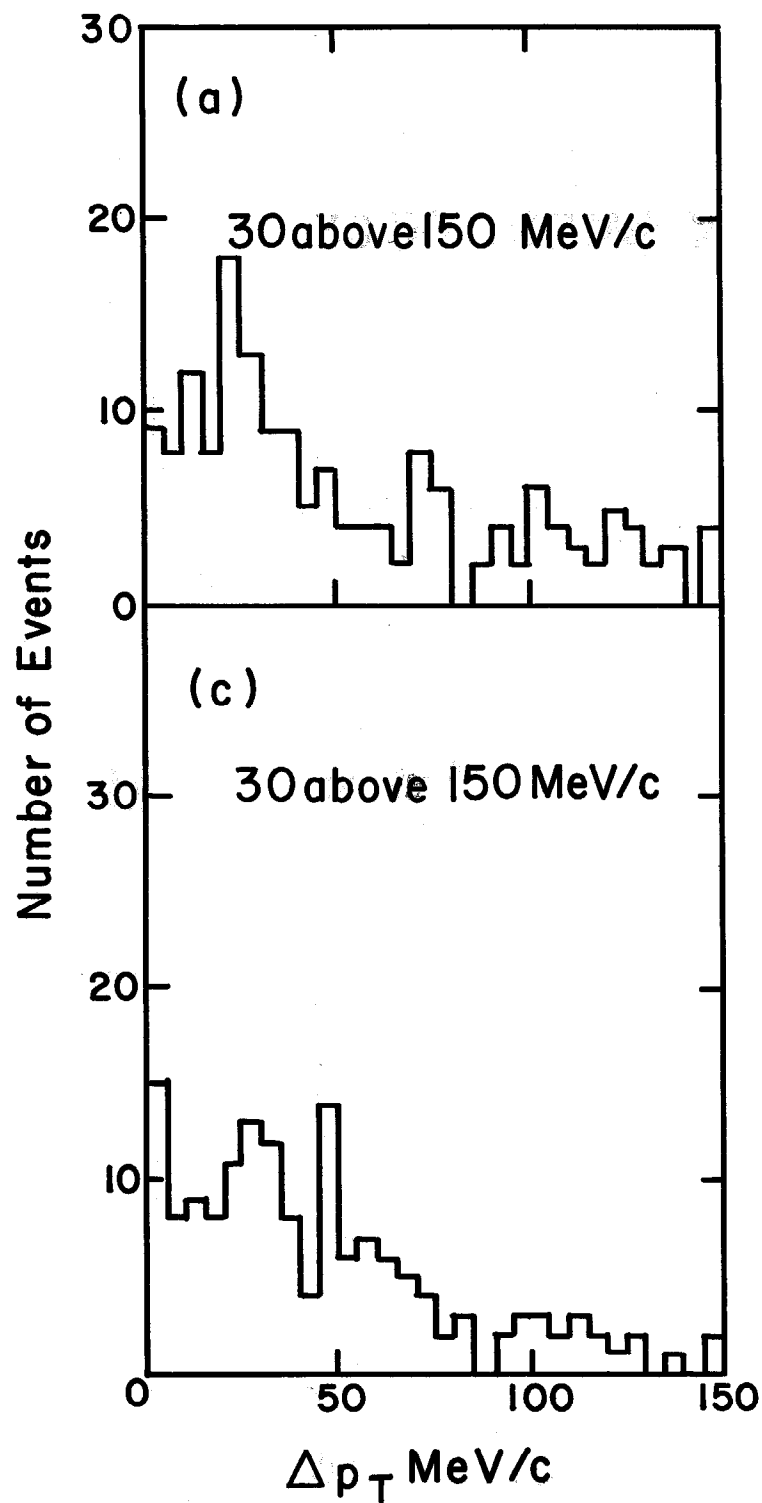


Fig. 5. Same as Fig. 4, except K^- -p scattering at 200 GeV/c.

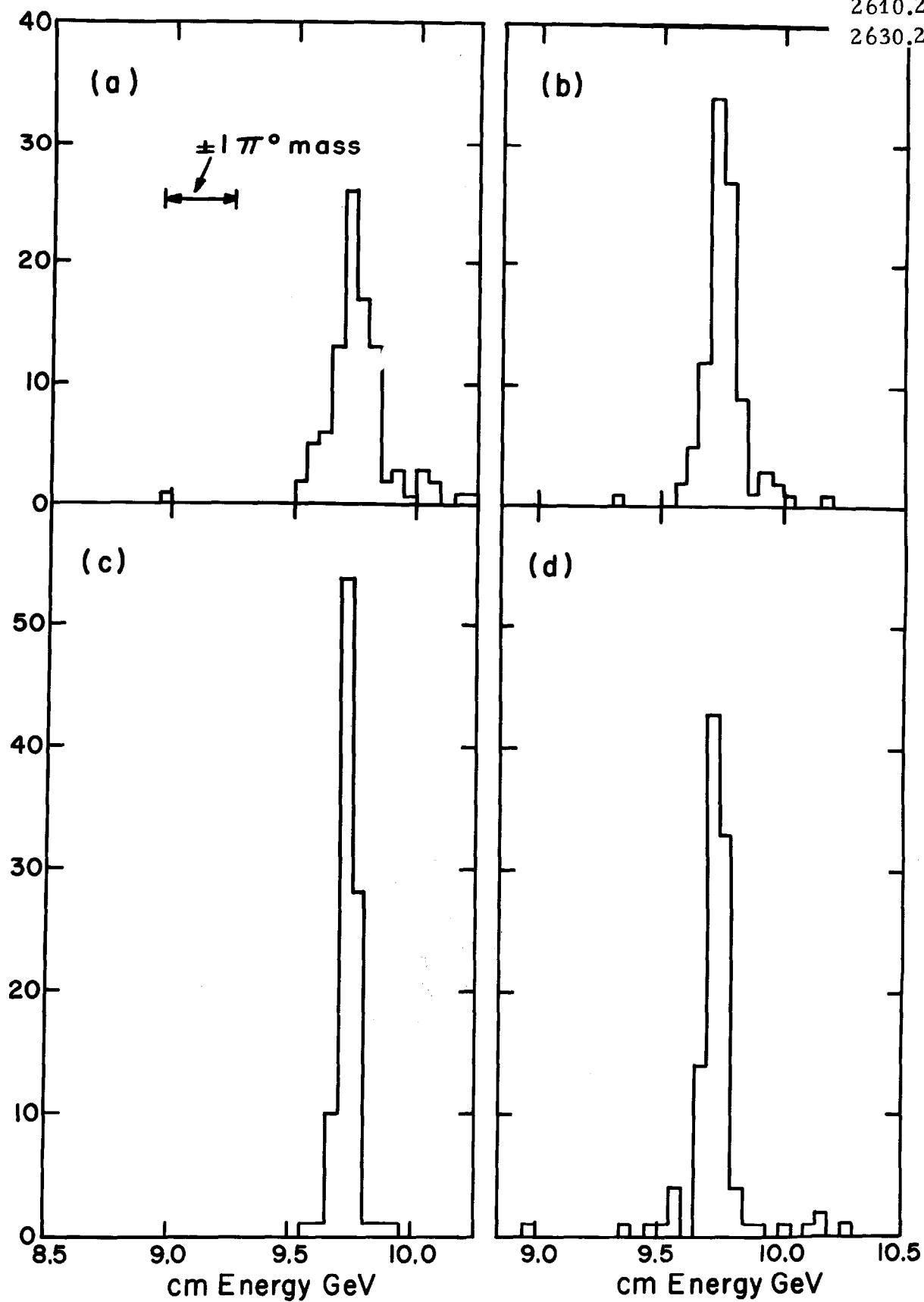


Fig. 6. Resolution in measuring total cm energy, K^-p scattering at 50 GeV/c. Bubble chamber operating conditions as in Fig. 4.

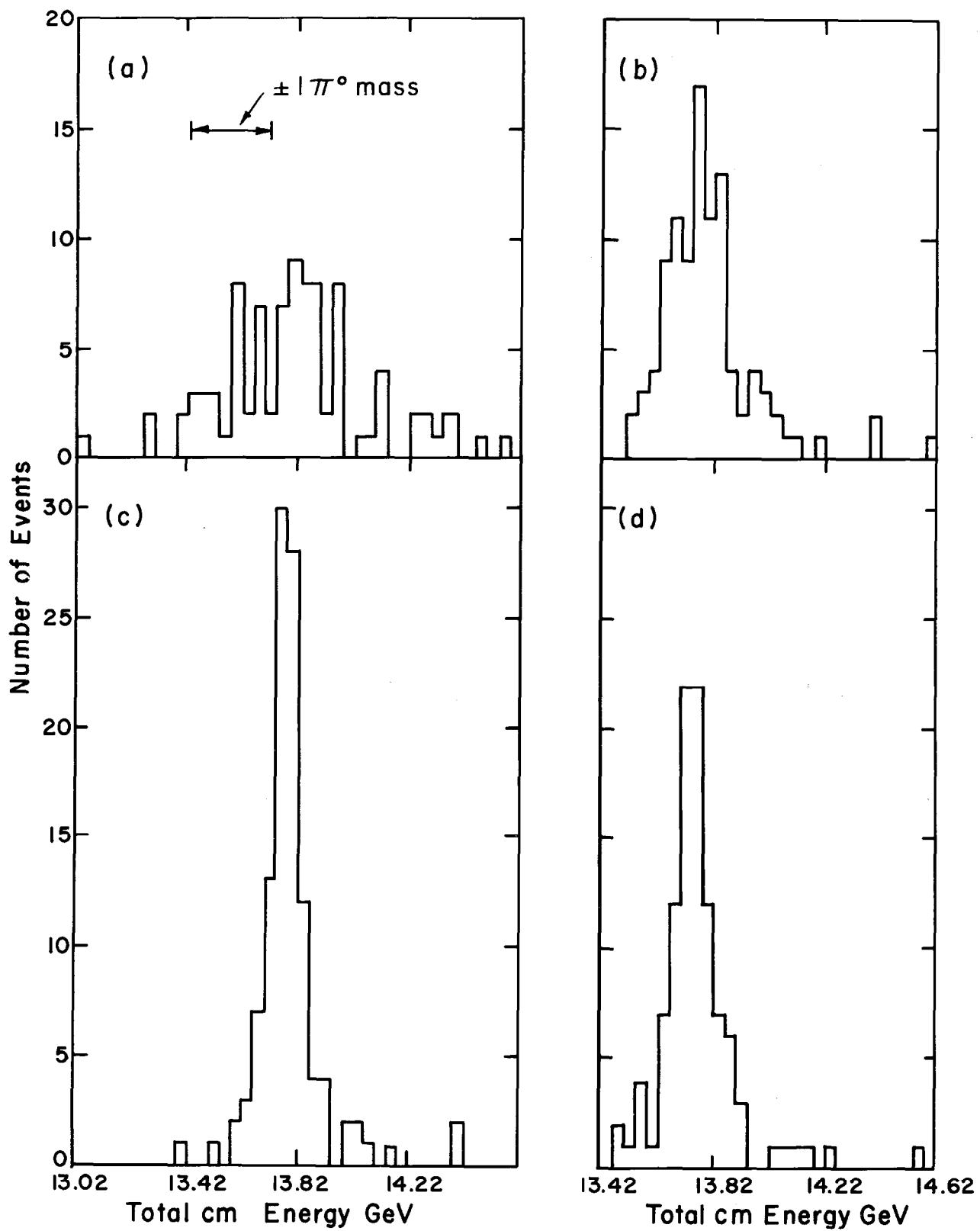


Fig. 7. Same as Fig. 6, at 100 GeV/c.

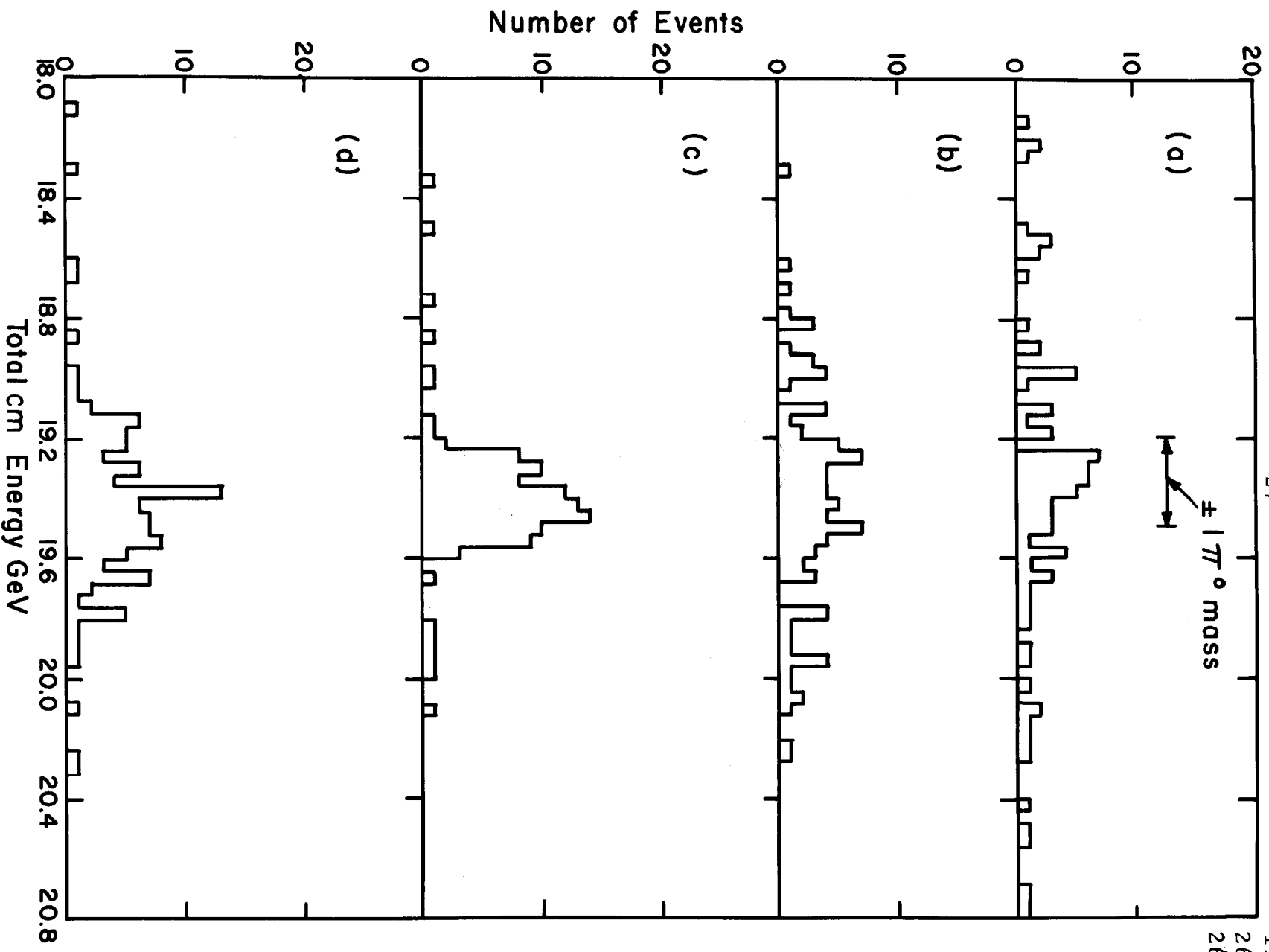


Fig. 8. Same as Fig. 6, at 200 GeV/c.

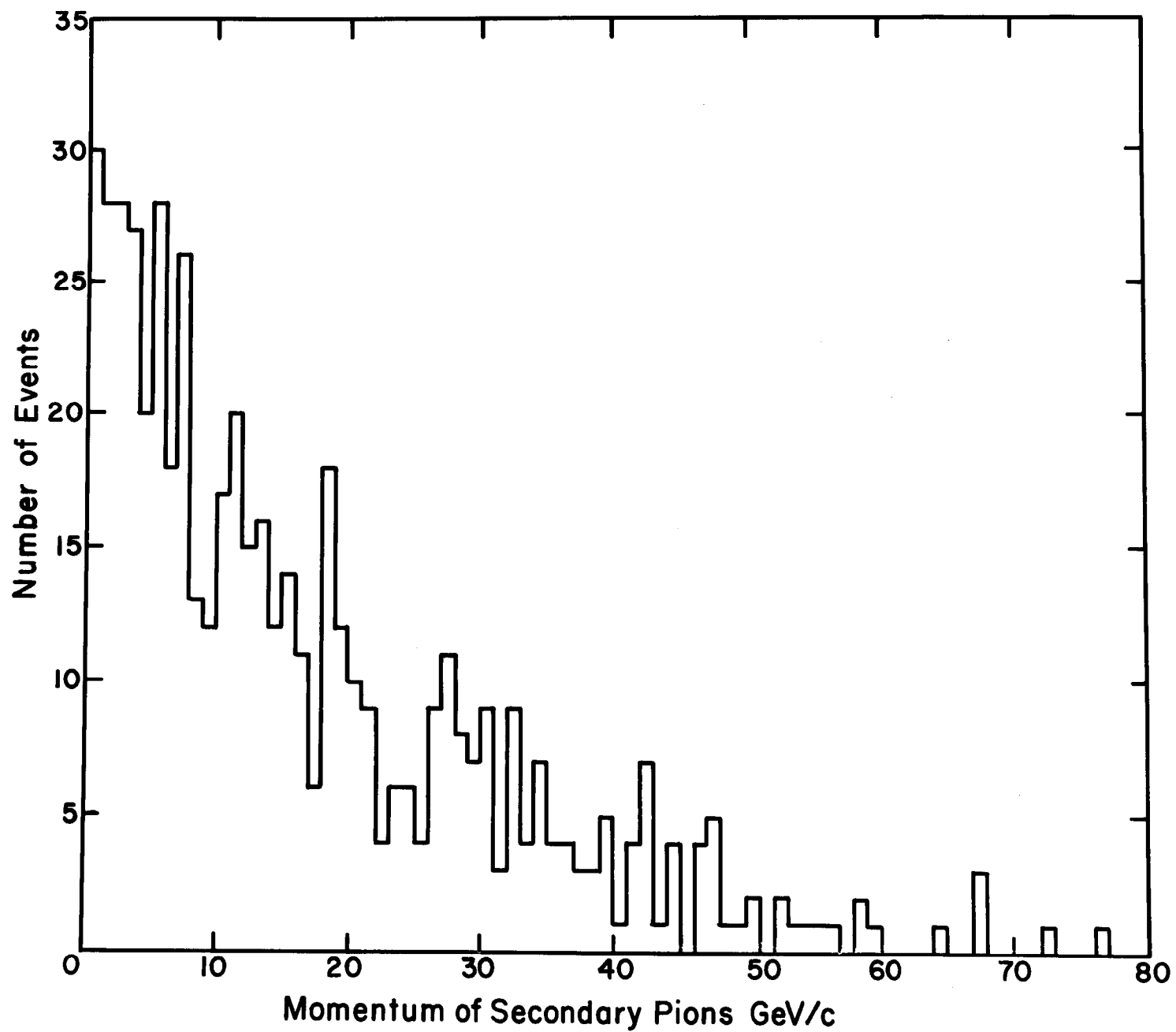


Fig. 9. Distribution of pion momenta given by FAKE for the reaction $\bar{p} + p \rightarrow 3\pi^+ 3\pi^-$ at 100 GeV/c.

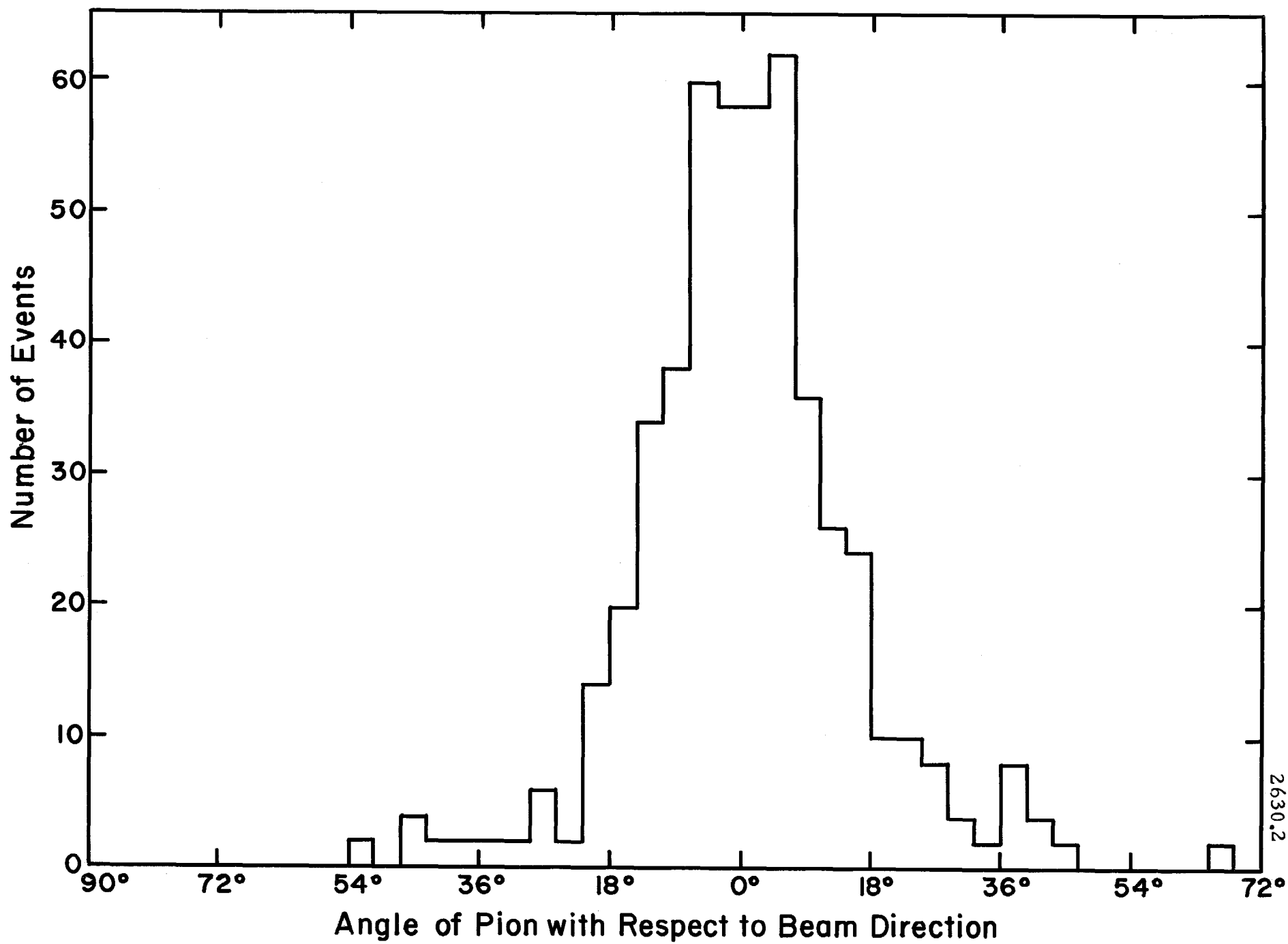


Fig. 10. Angular distribution of pions in the same reaction.

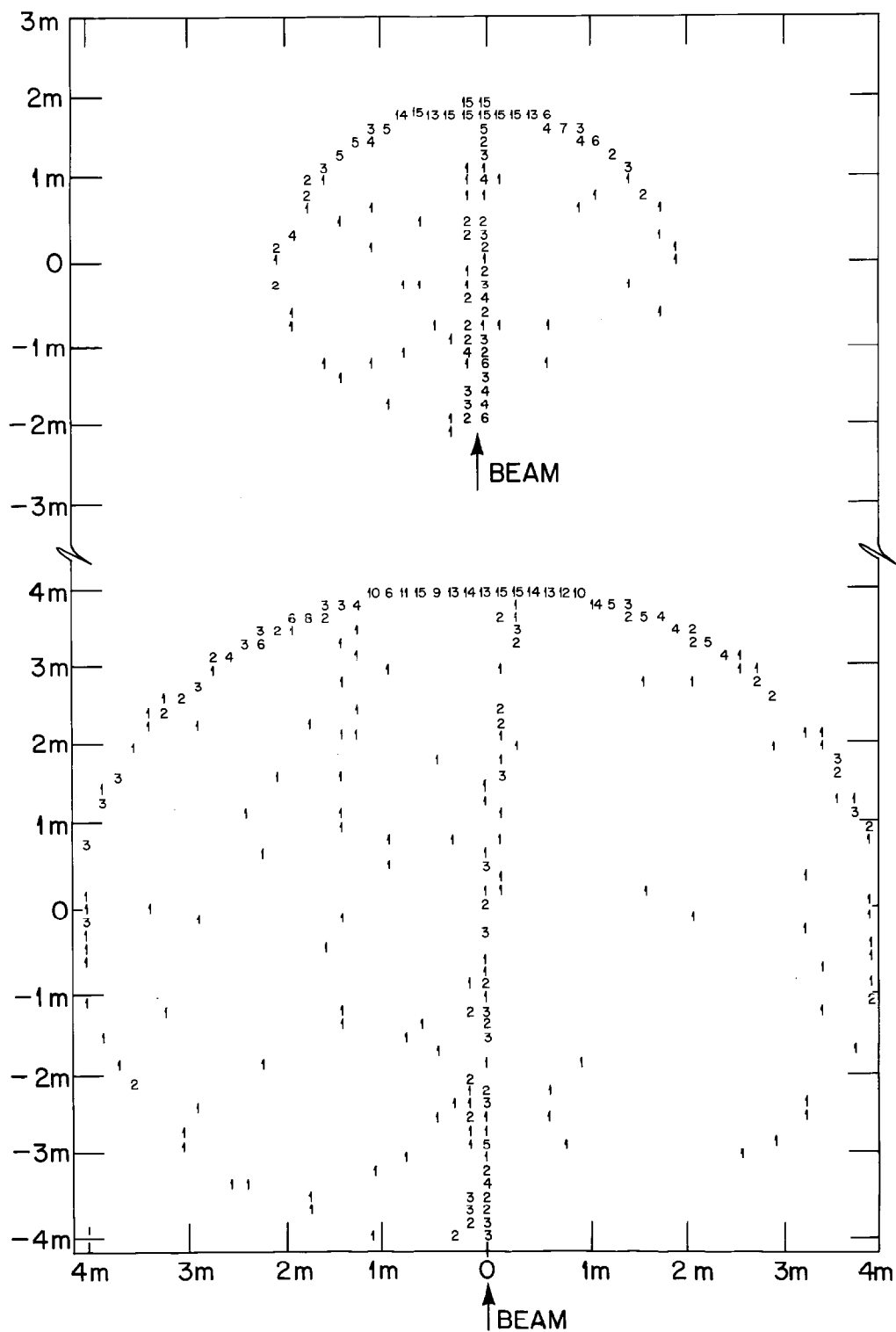


Fig. 11. End points of antiproton and pion tracks in the 12-ft and 25-ft chambers, at 40-kG field. Reaction is $p\bar{p} \rightarrow 3\pi^+ 3\pi^-$ at 100 GeV/c.

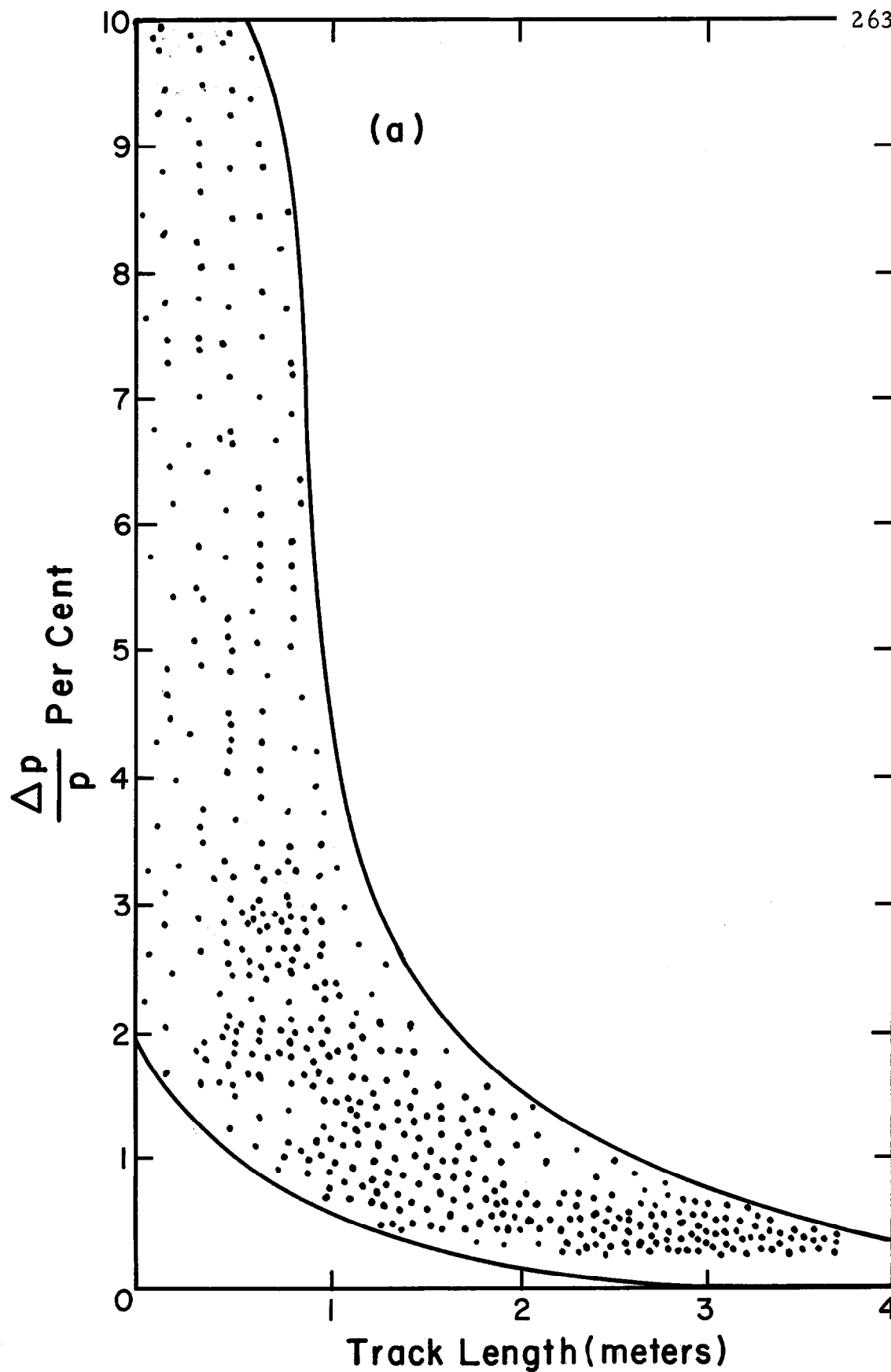


Fig. 12a. FAKE-generated scatter diagram of momentum error vs. track length for the annihilation reaction $\bar{p} + p \rightarrow 3\pi^+ 3\pi^-$ at 50 GeV/c. This plot is for the ANL 12-ft. chamber, 20 kg field, $\epsilon = 250\mu$.

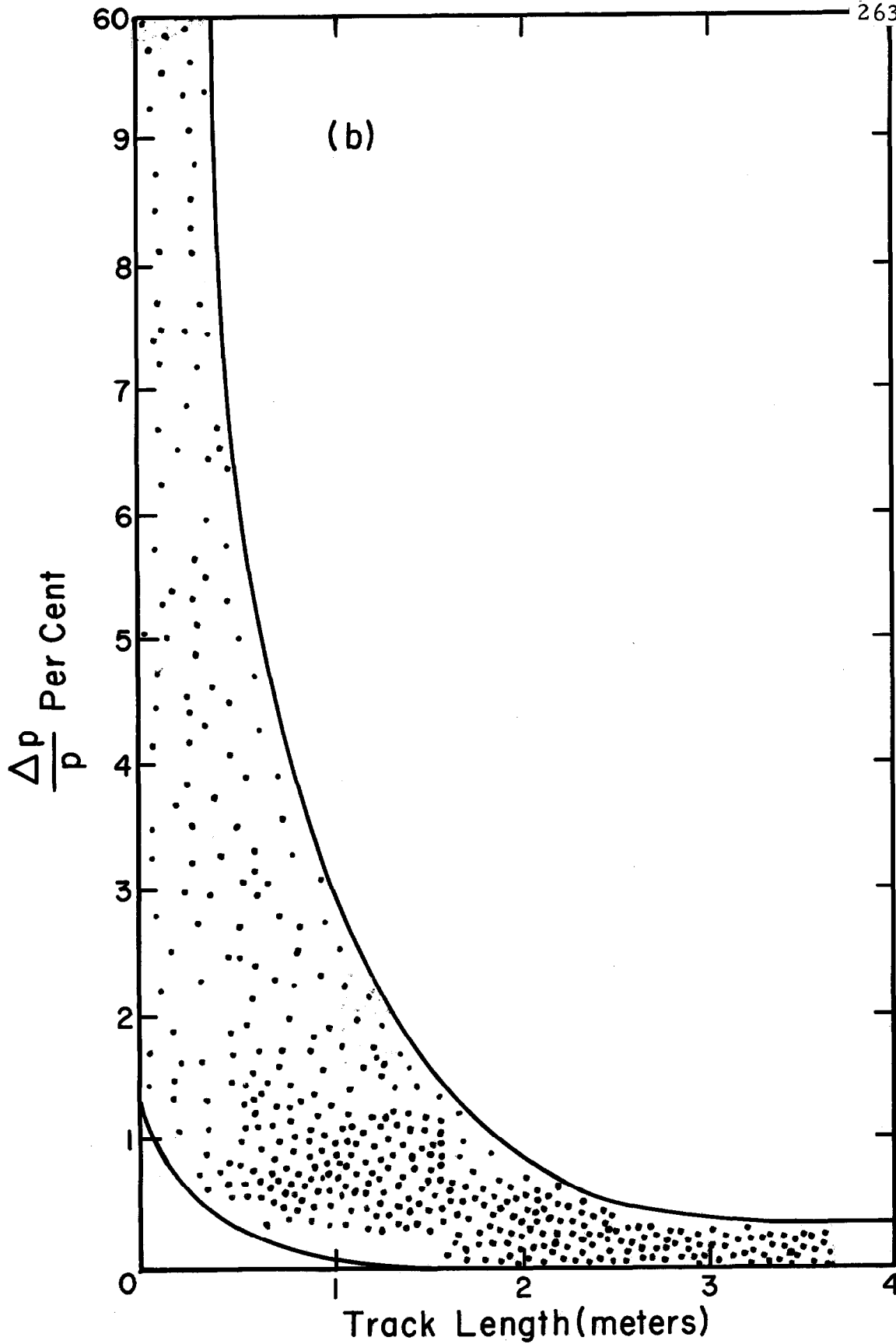


Fig. 12b.. Same as 12a, with 40 kgauss field.

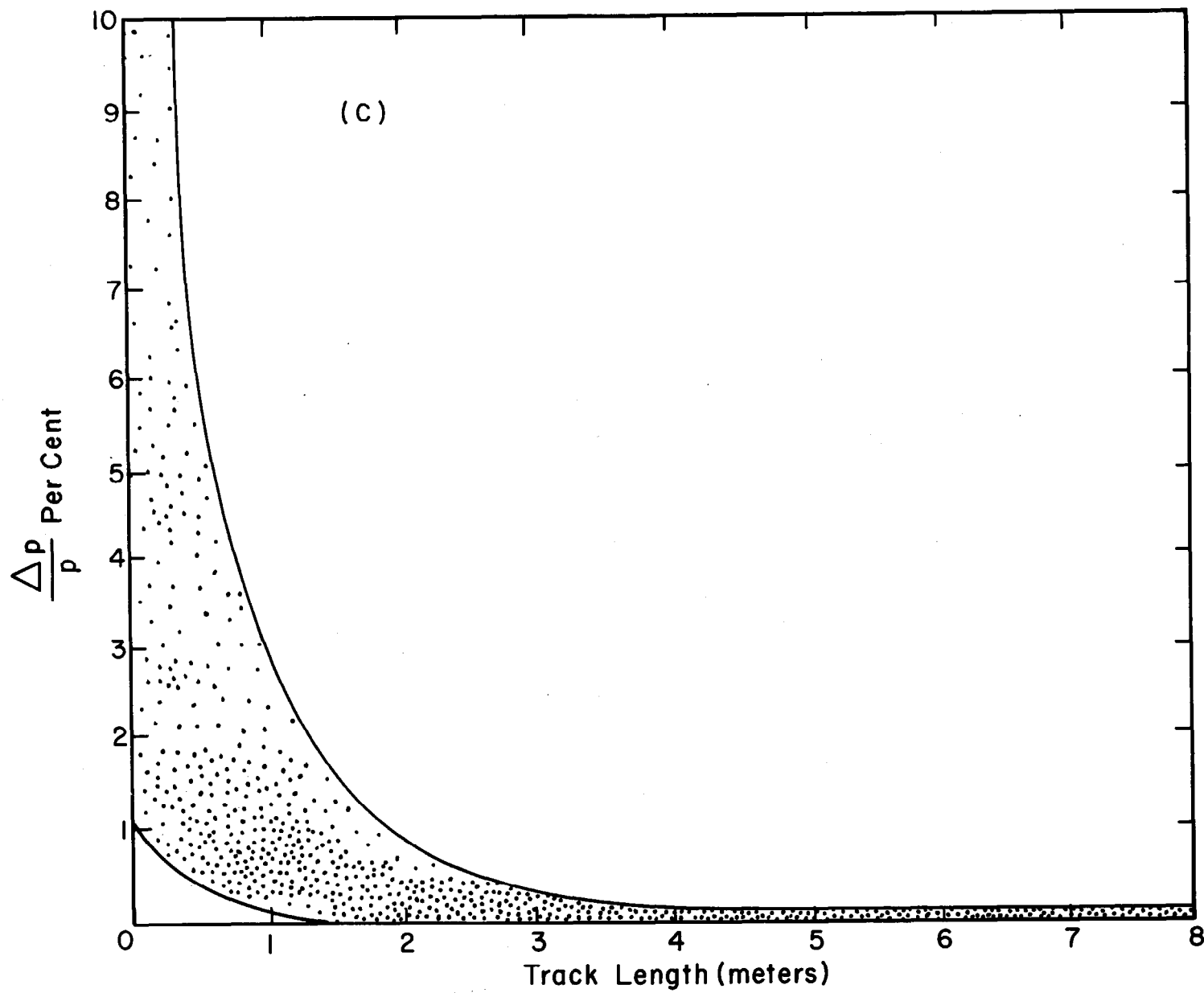


Fig. 12c. Same as 12a, for 25-ft. chamber, 40 kgauss, $\epsilon = 250\mu$.

TM-151
 2610.2
 2630.2
 -33-

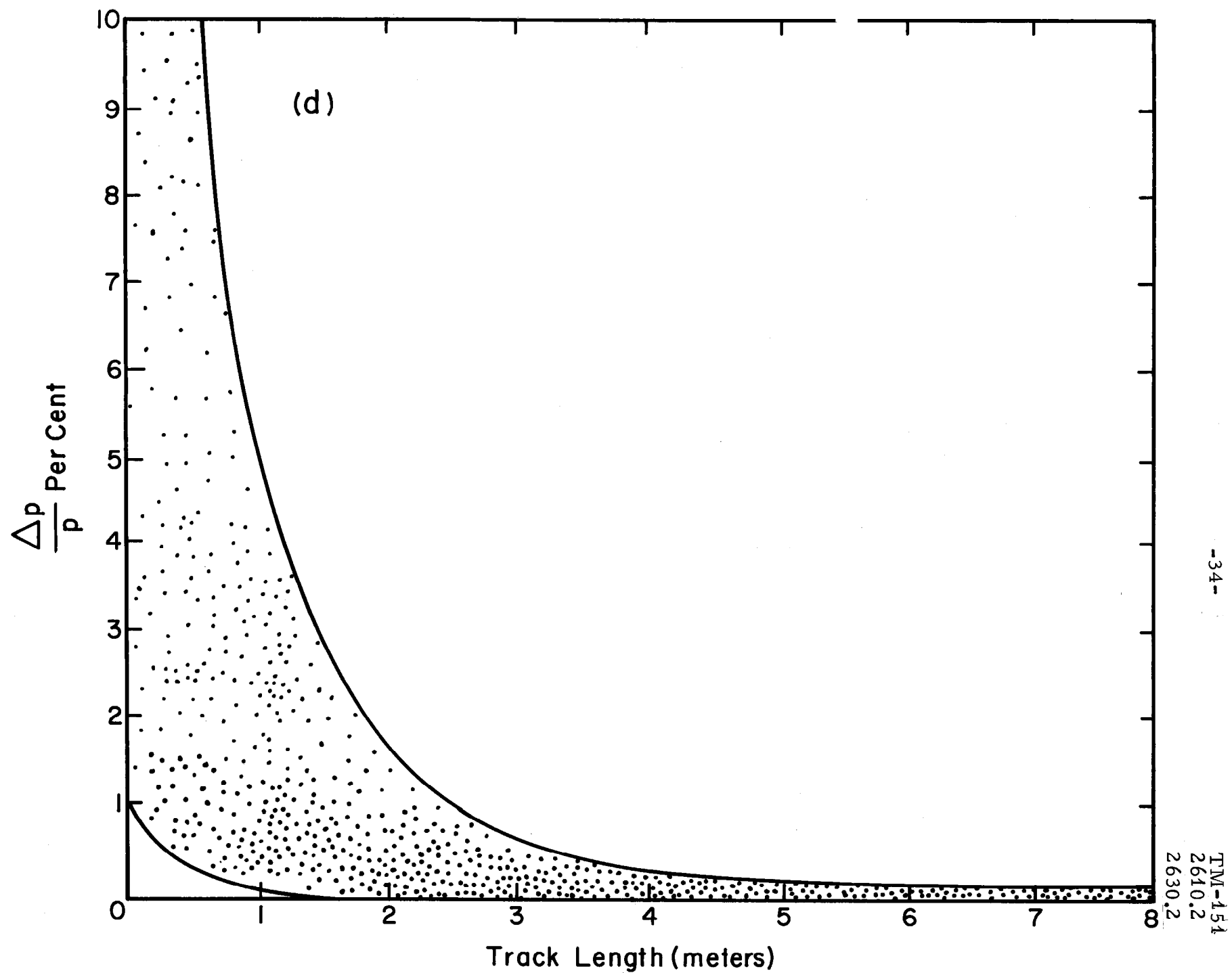


Fig. 12d. Same as 12c, with $\epsilon = 500\mu$

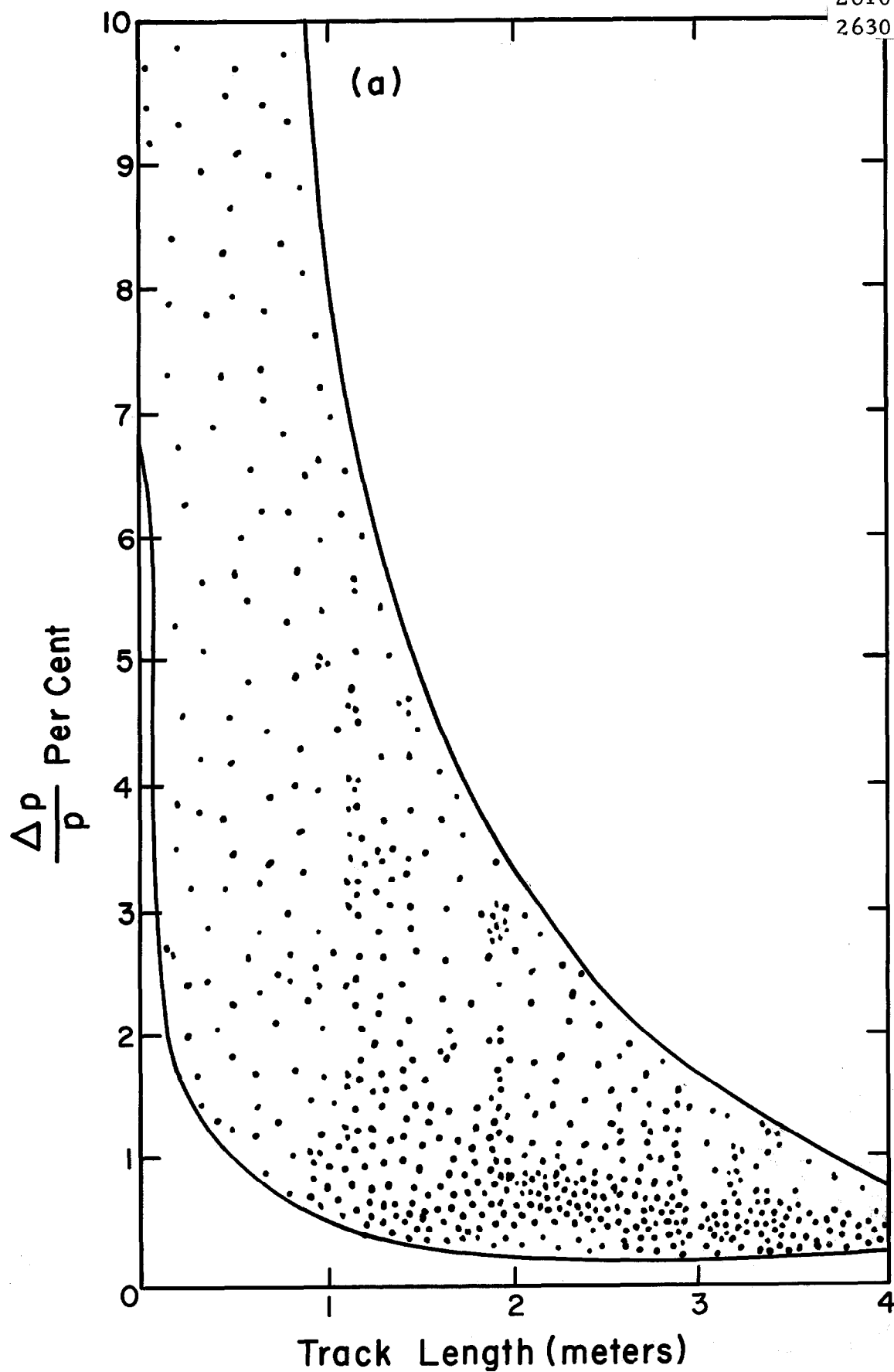


Fig. 13a. Same as Fig. 12a, with annihilation at 100 Gev/c.

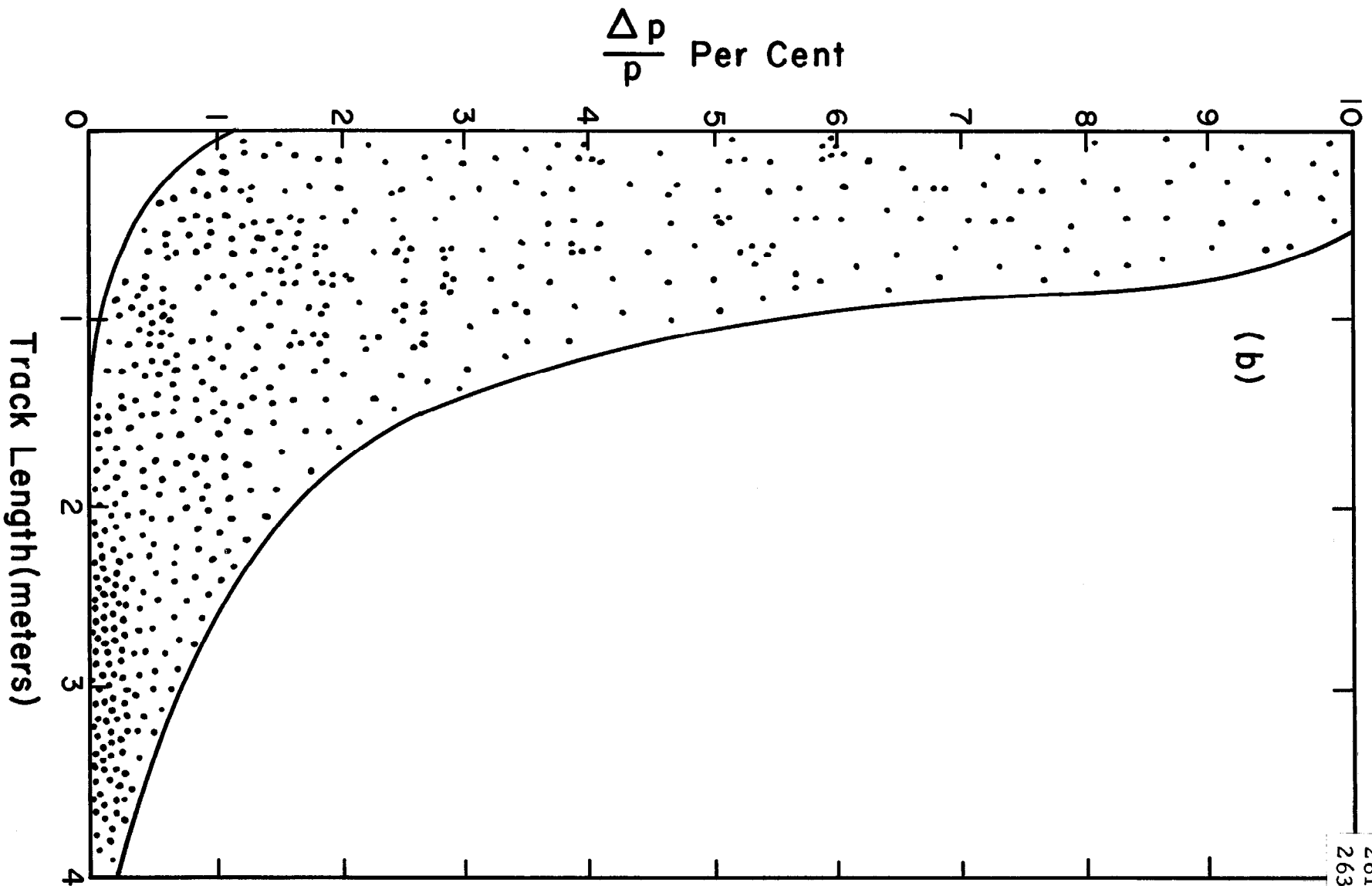


Fig. 13b. Same as 12b, reaction at 100 Gev/c.

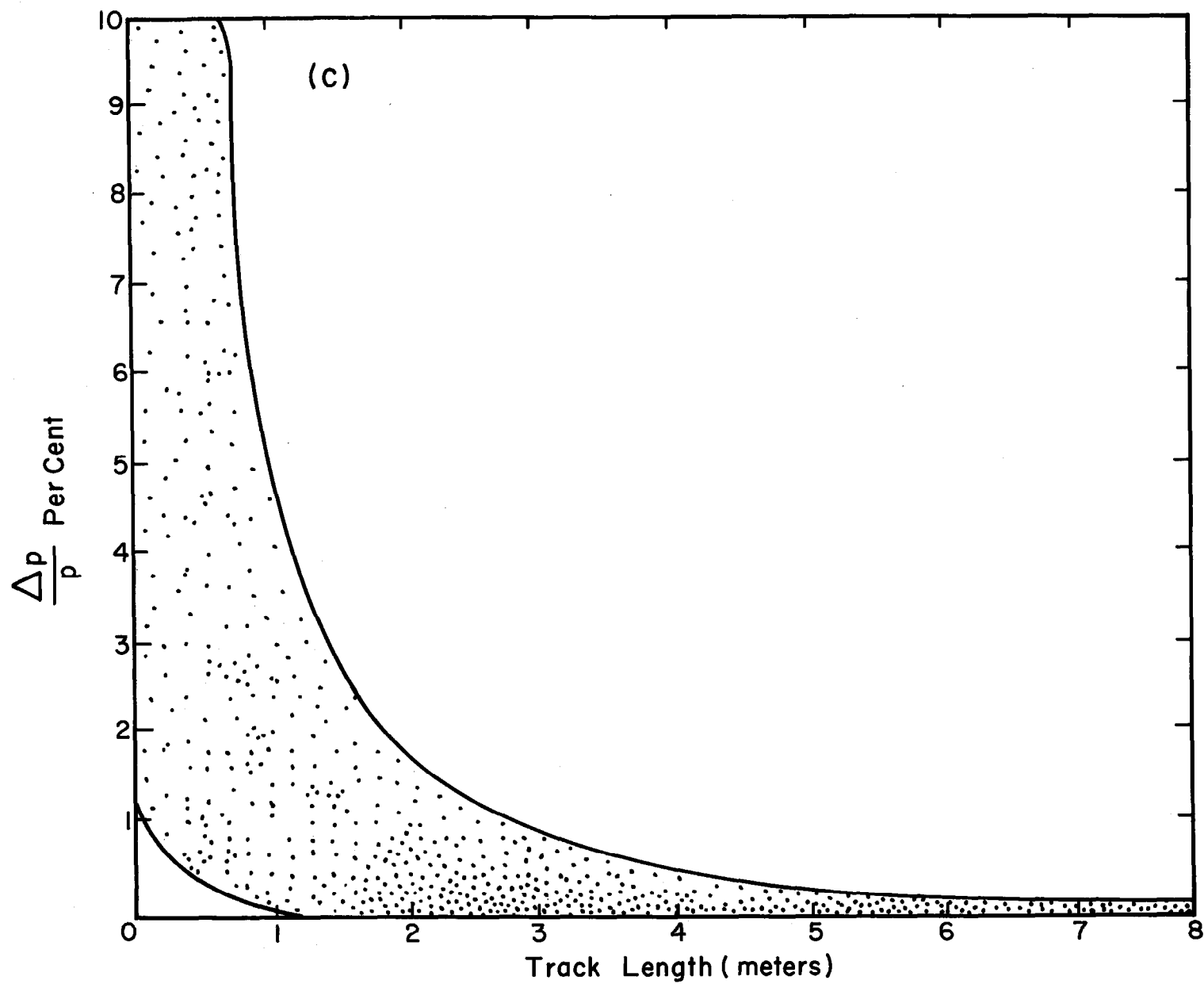


Fig. 13c. Same as 12c, reaction at 100 GeV/c.

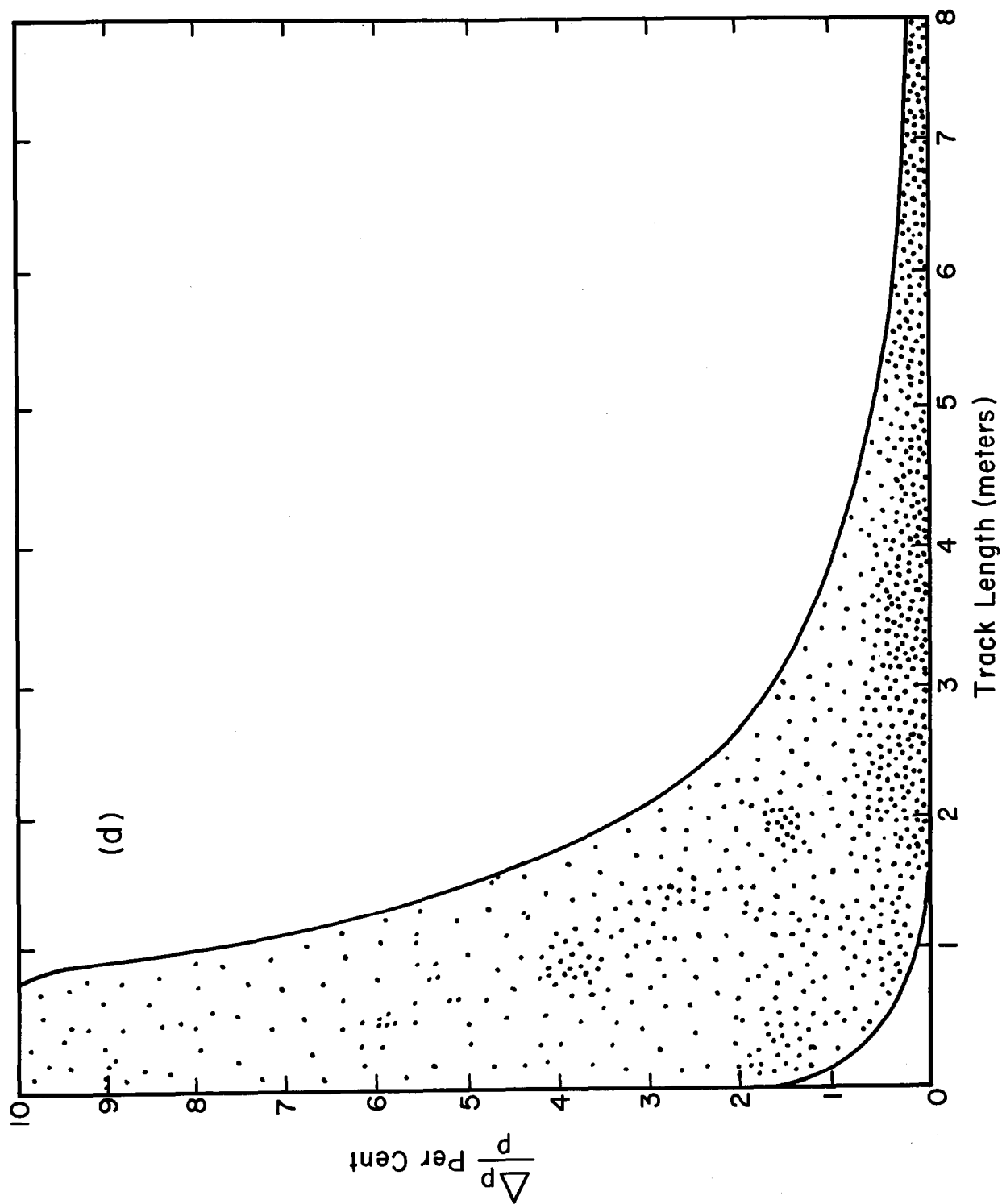


Fig. 13d. Same as 12d, reaction at 100 GeV/c.

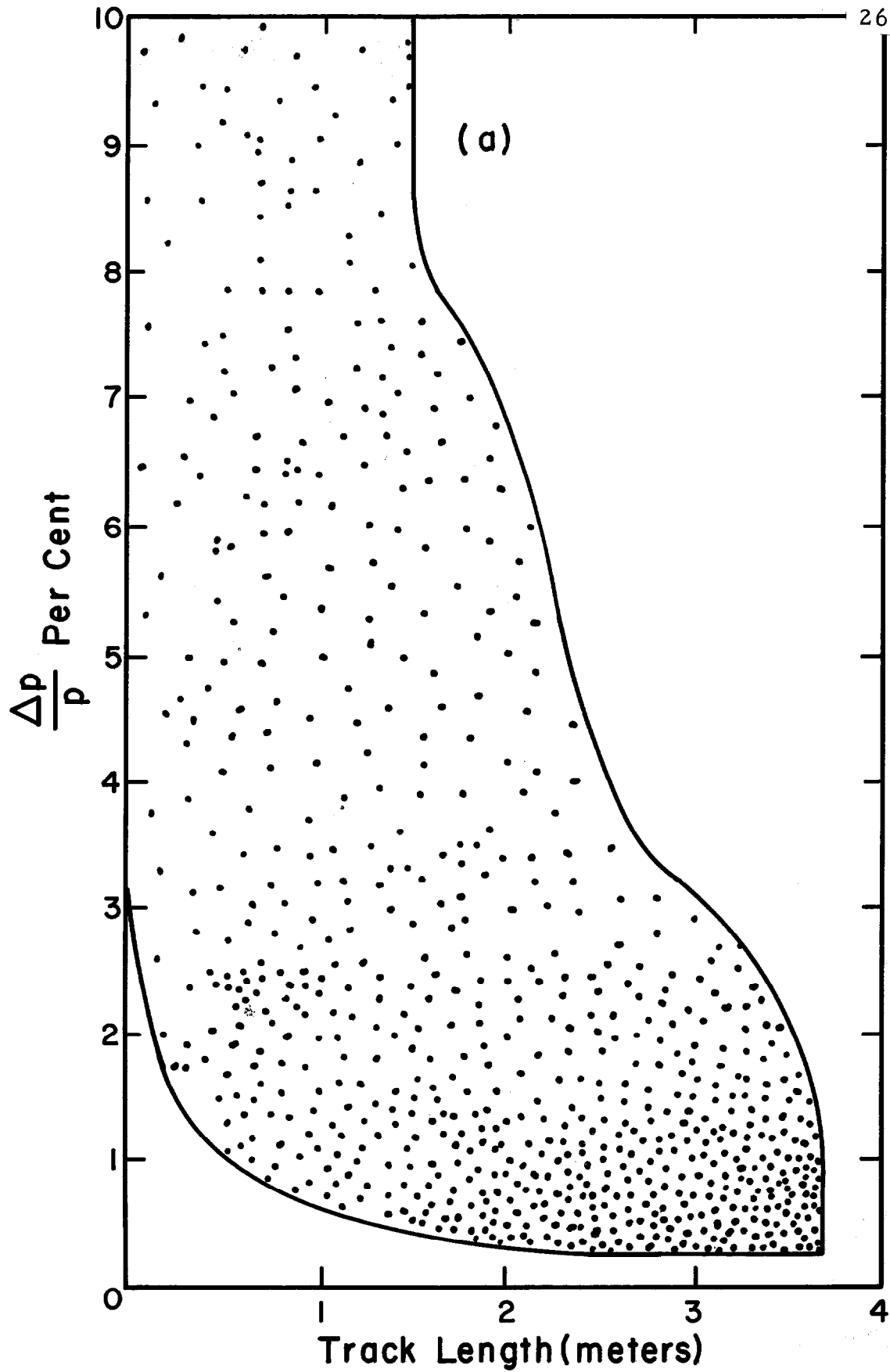


Fig. 14a. Same as Fig. 12a, with reaction at 200 Gev/c.

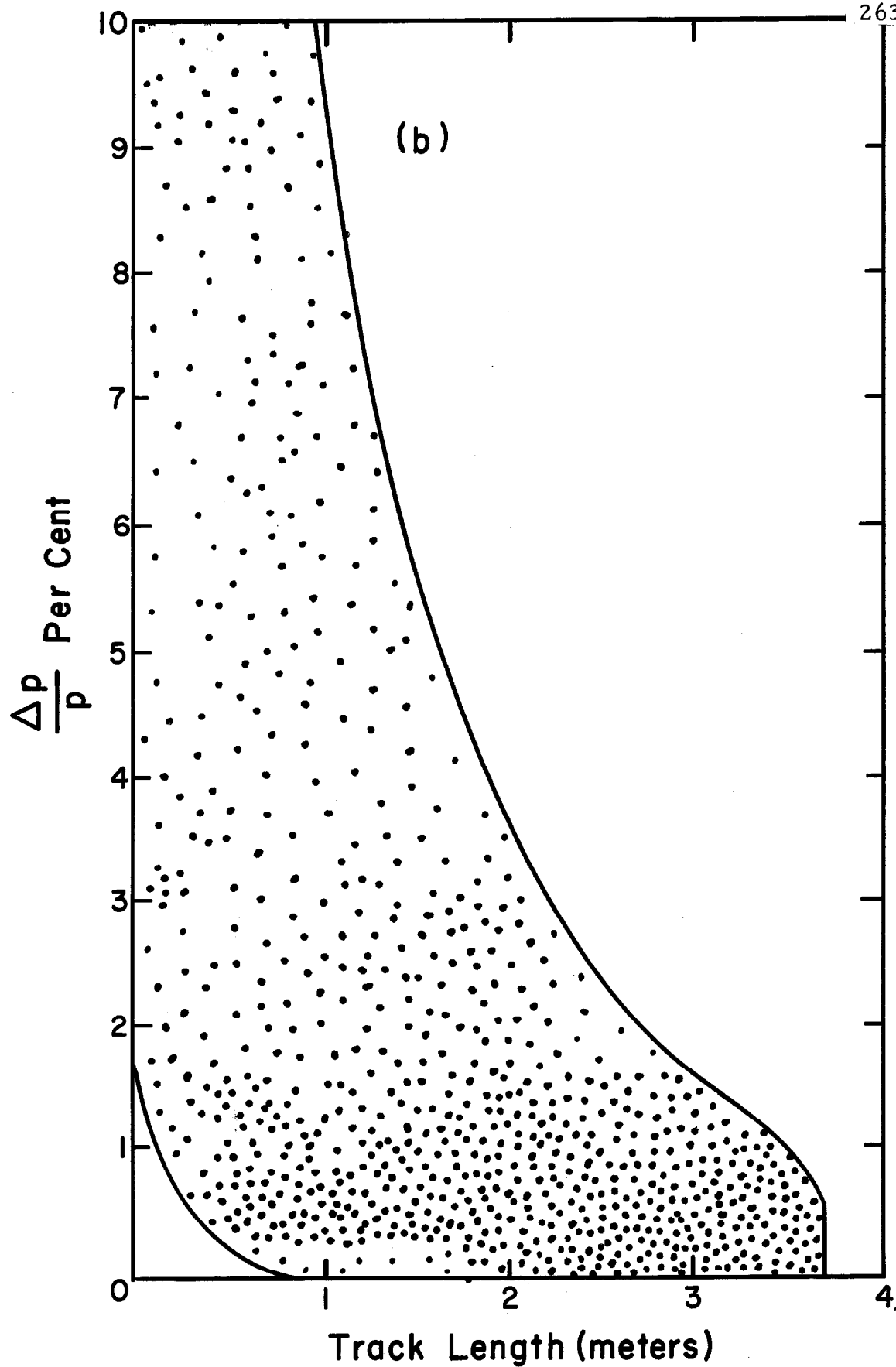


Fig. 14b. Same as 12b, reaction at 200 Gev/c.

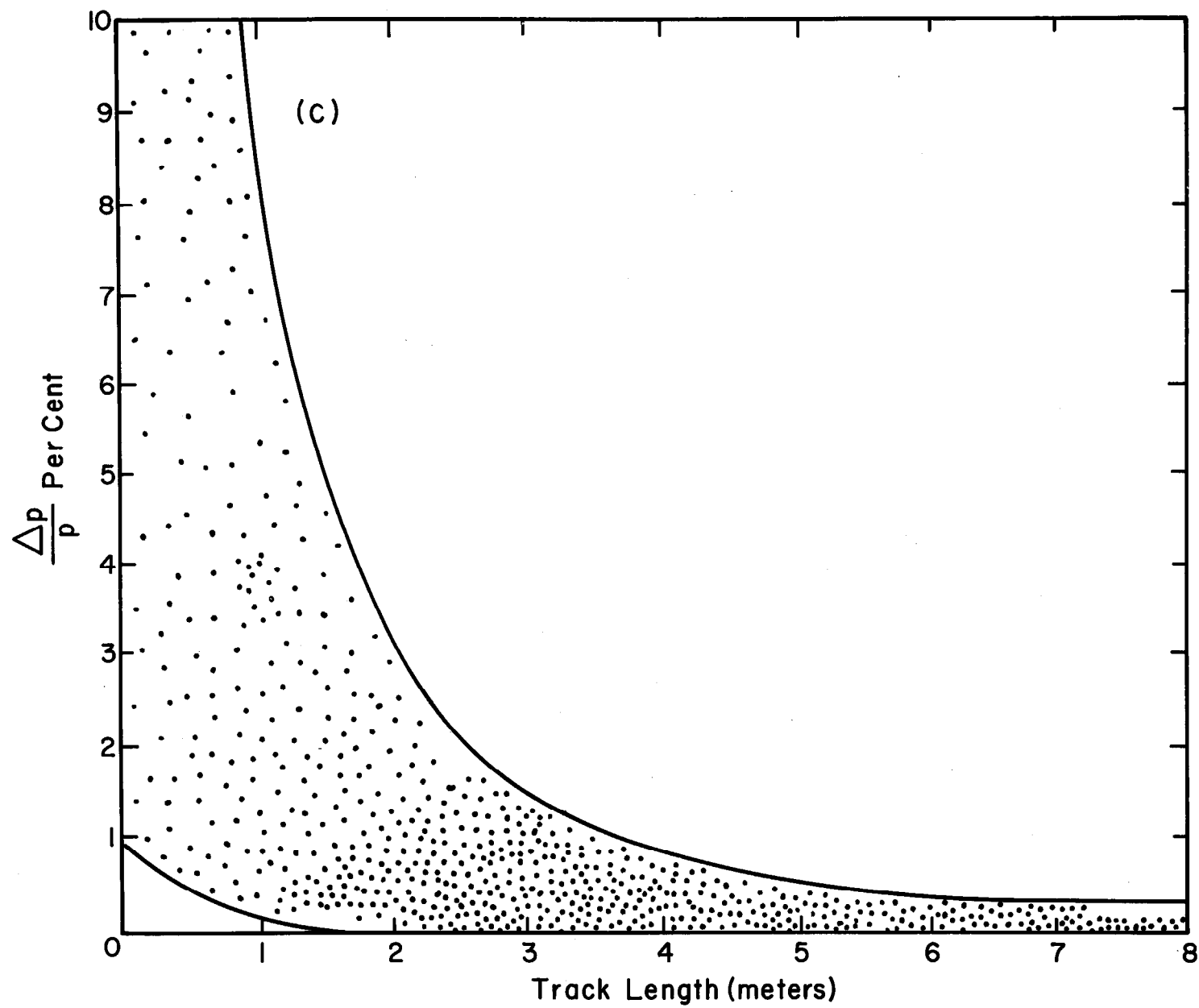


Fig. 14c. Same as 12c, reaction at 200 Gev/c.

TM-151
2610.2
2630.2

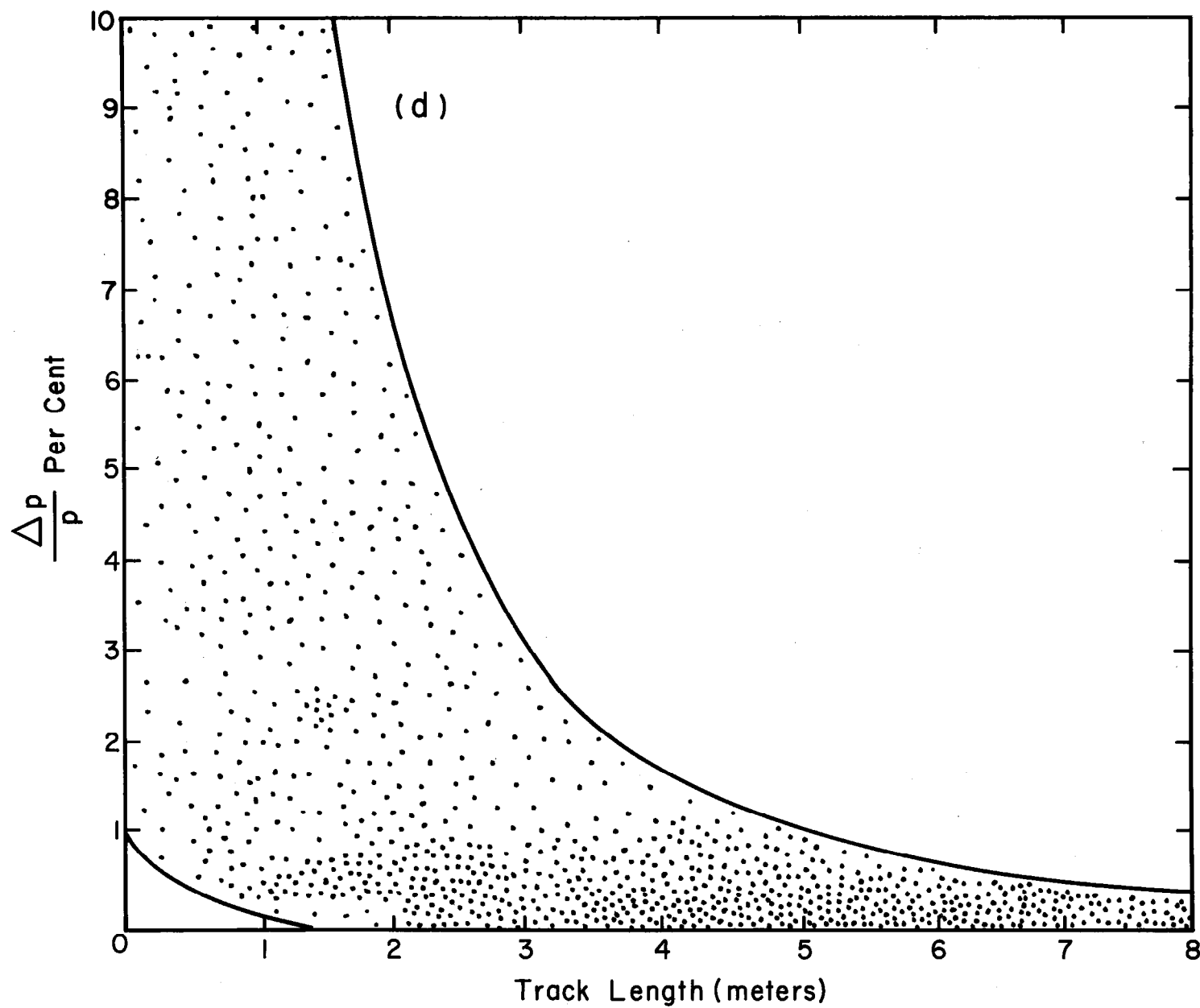


Fig. 14d. Same as 12d, reaction at 200 Gev/c.

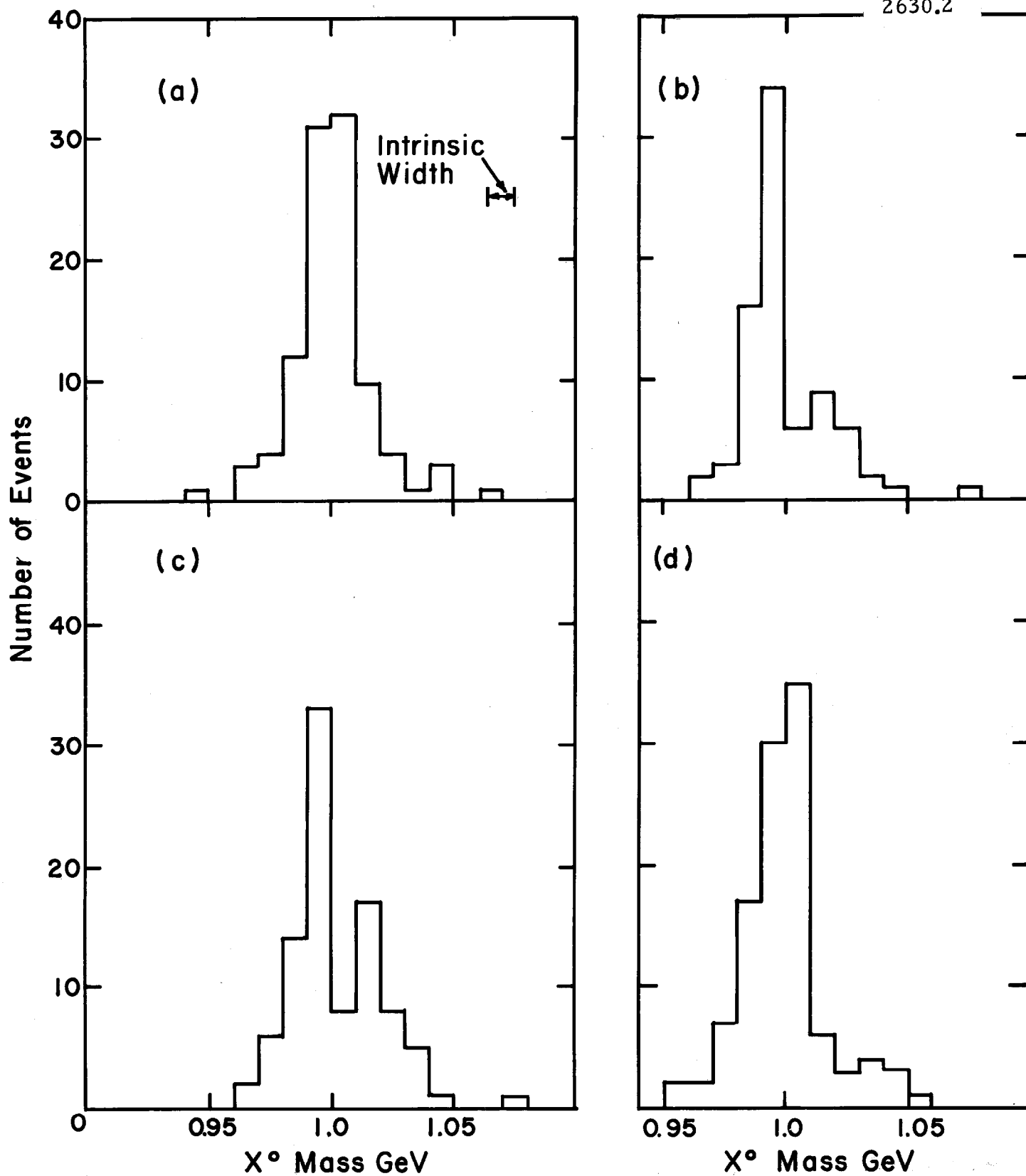


Fig. 15. Mass Resolution for missing mass X^0 observed in the reaction $\bar{p} + p \rightarrow 2\pi^+ 2\pi^- X^0$, with subsequent decay $X^0 \rightarrow \pi^+ \pi^-$, at 50 GeV/c. 15a-d, bubble chamber operating conditions as in previous curves, e.g. Fig. 4.

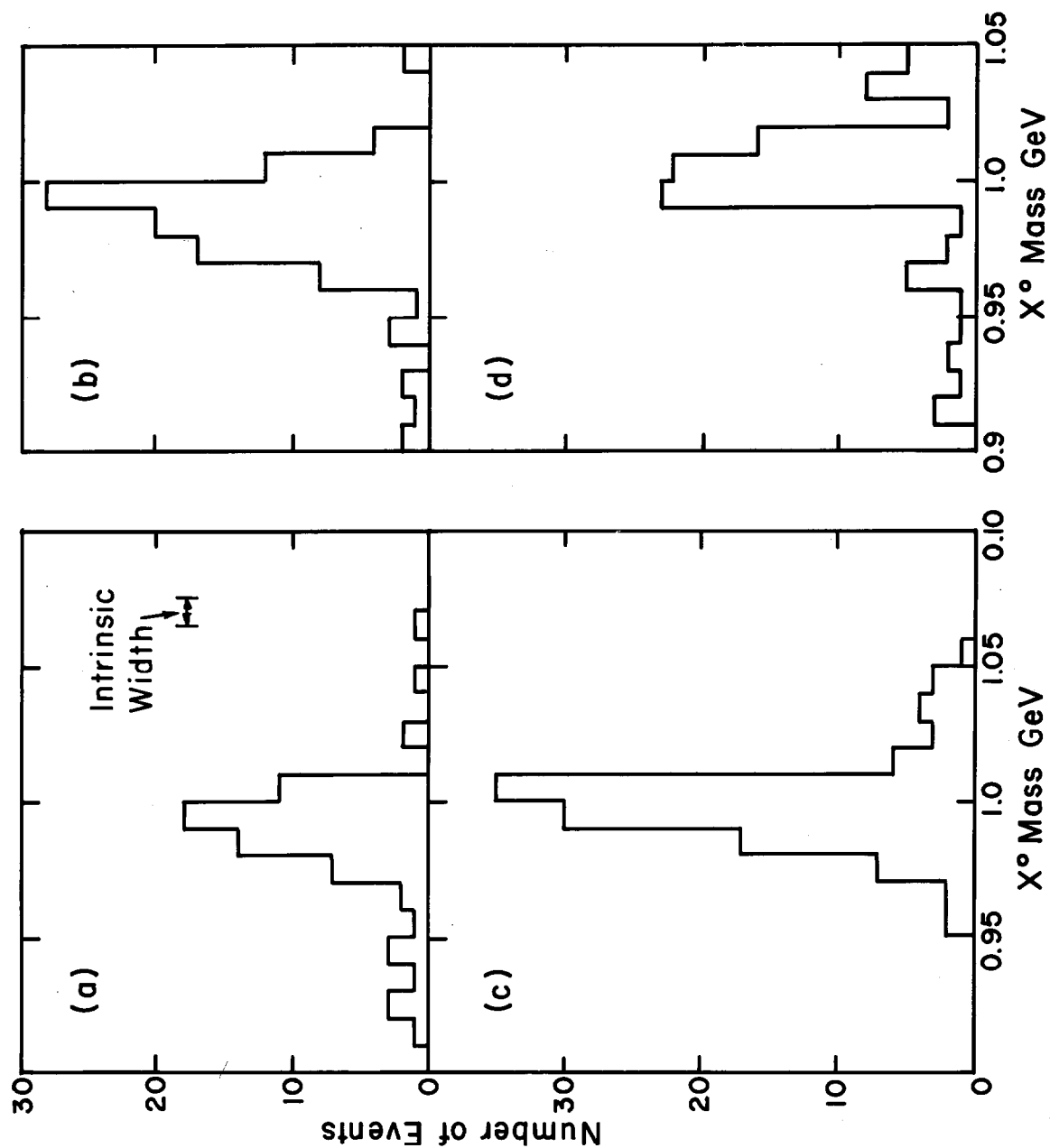


Fig. 16. Same as Fig. 15, except at 200 GeV/c.

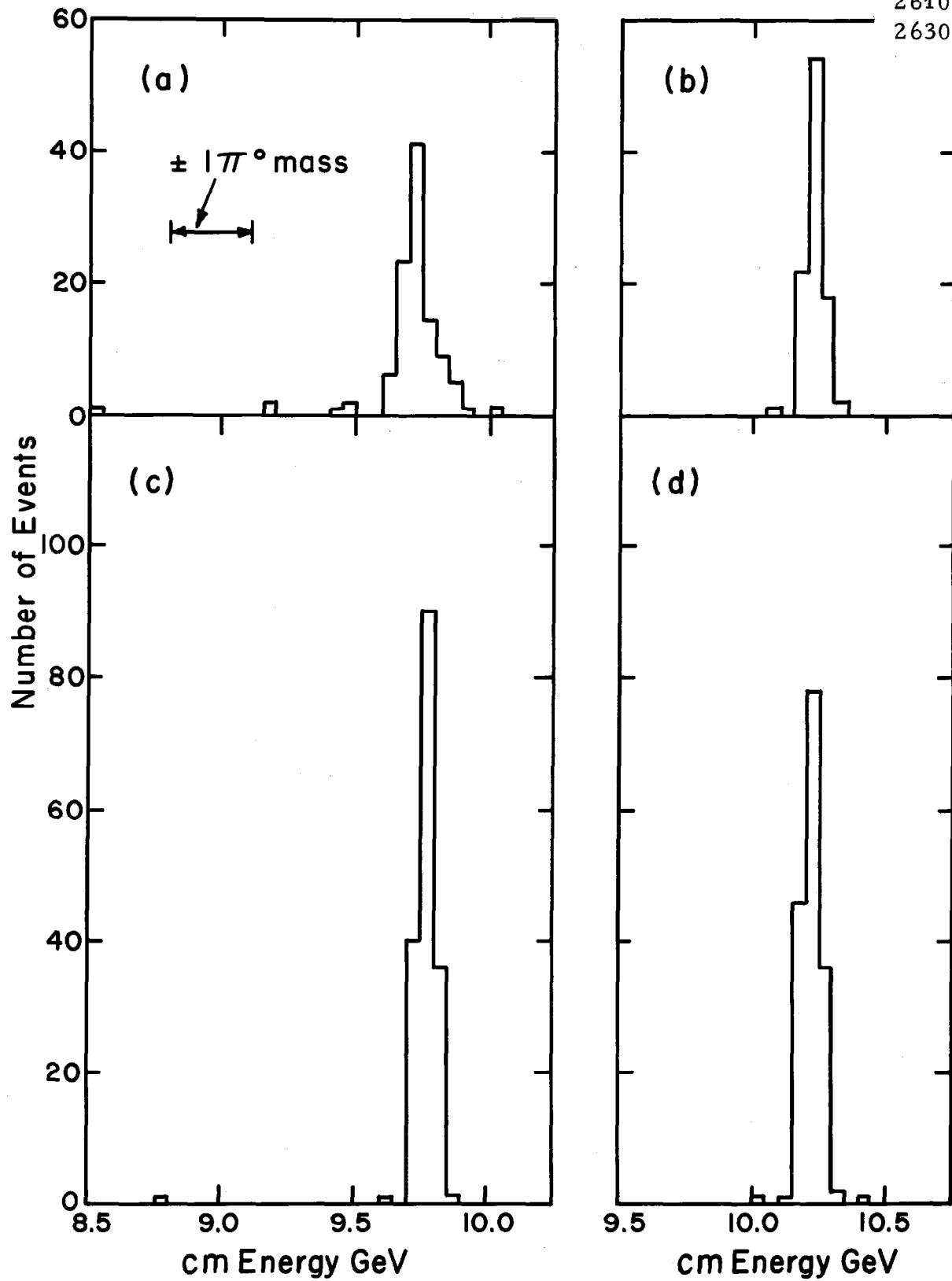


Fig. 17. Resolution of cm energy, same reaction as Fig. 9, at 50 GeV/c.

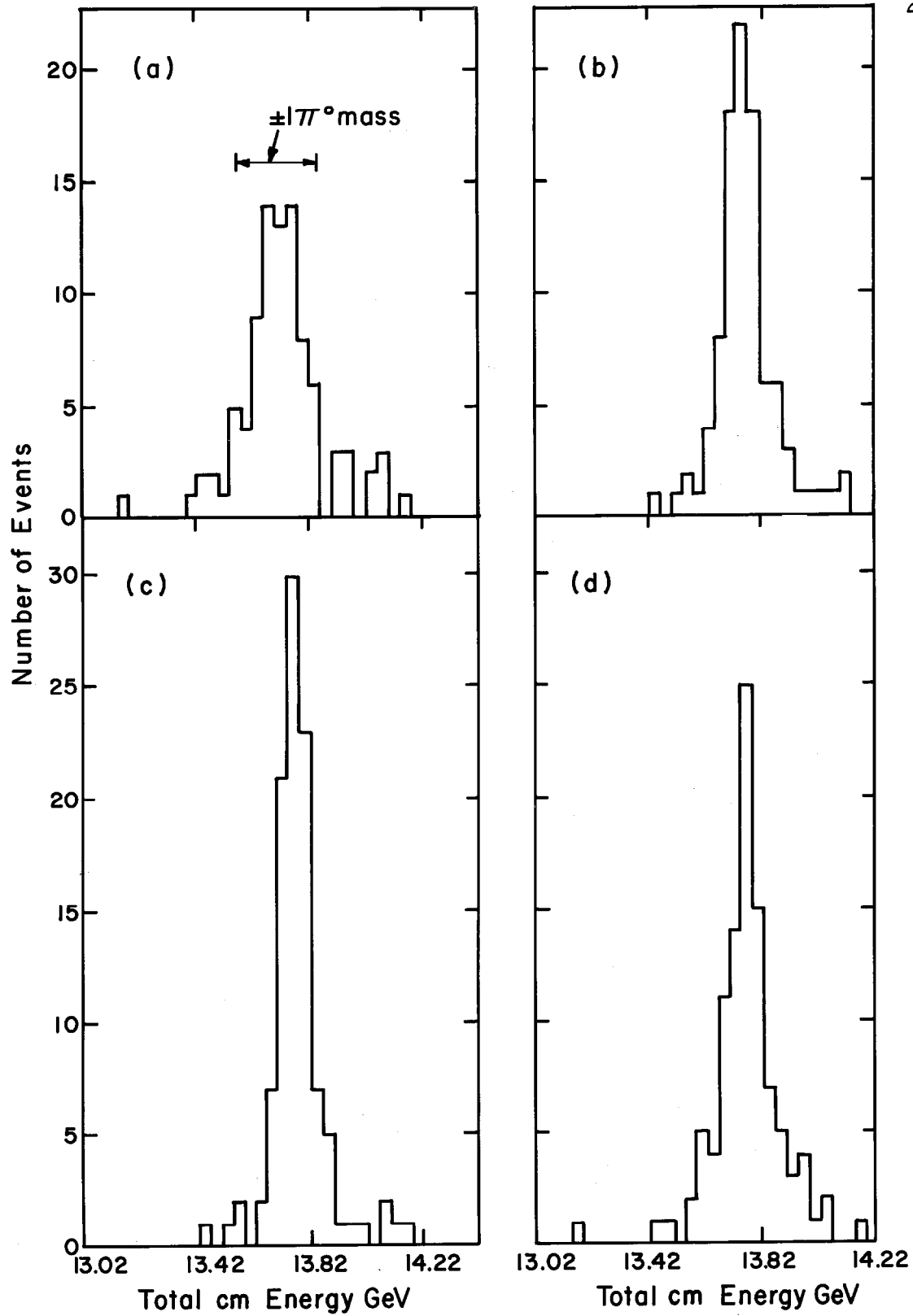


Fig. 18. Same as Fig. 17, at 100 GeV/c.

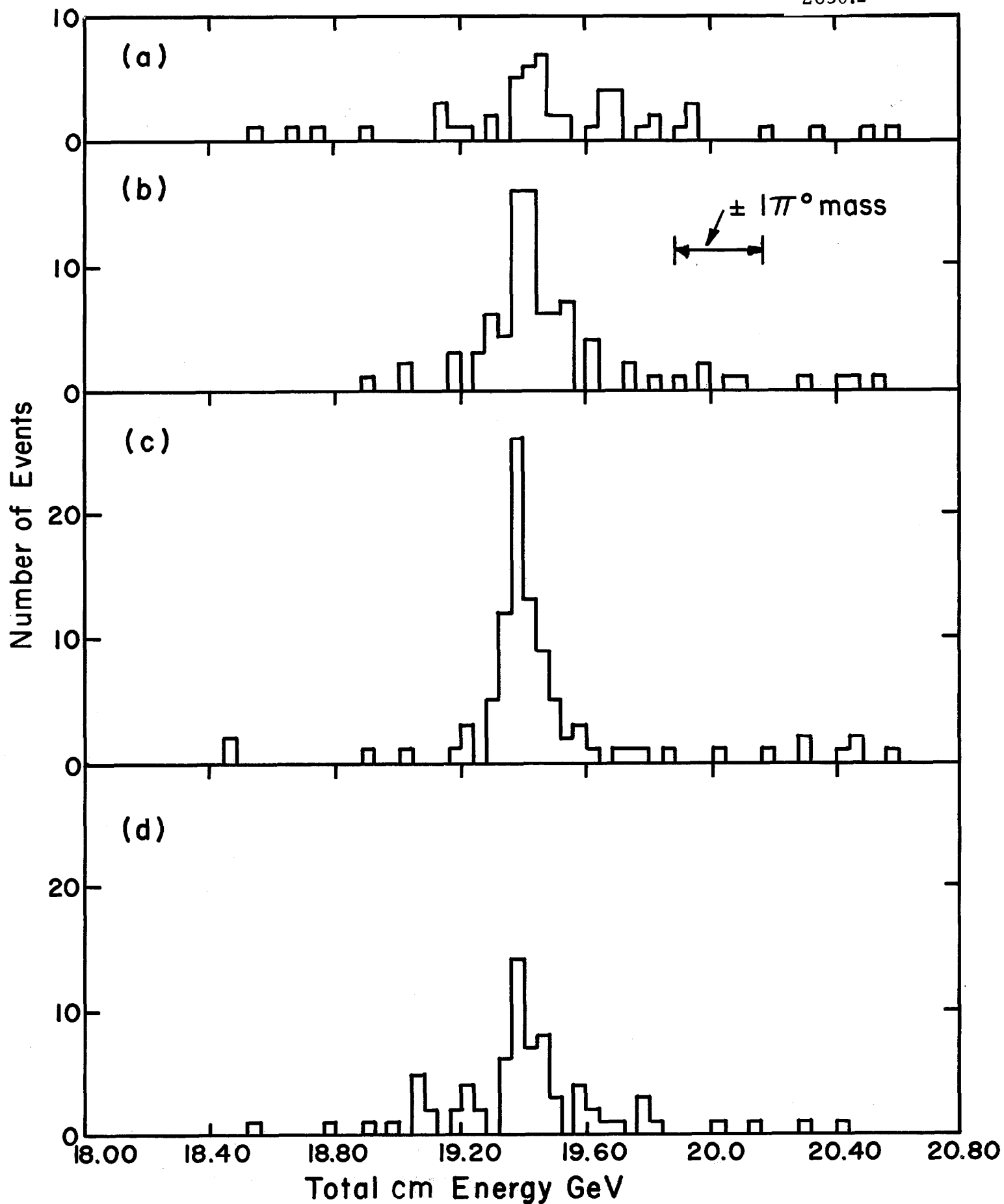


Fig. 19. Same as Fig. 17, at 200 GeV/c.

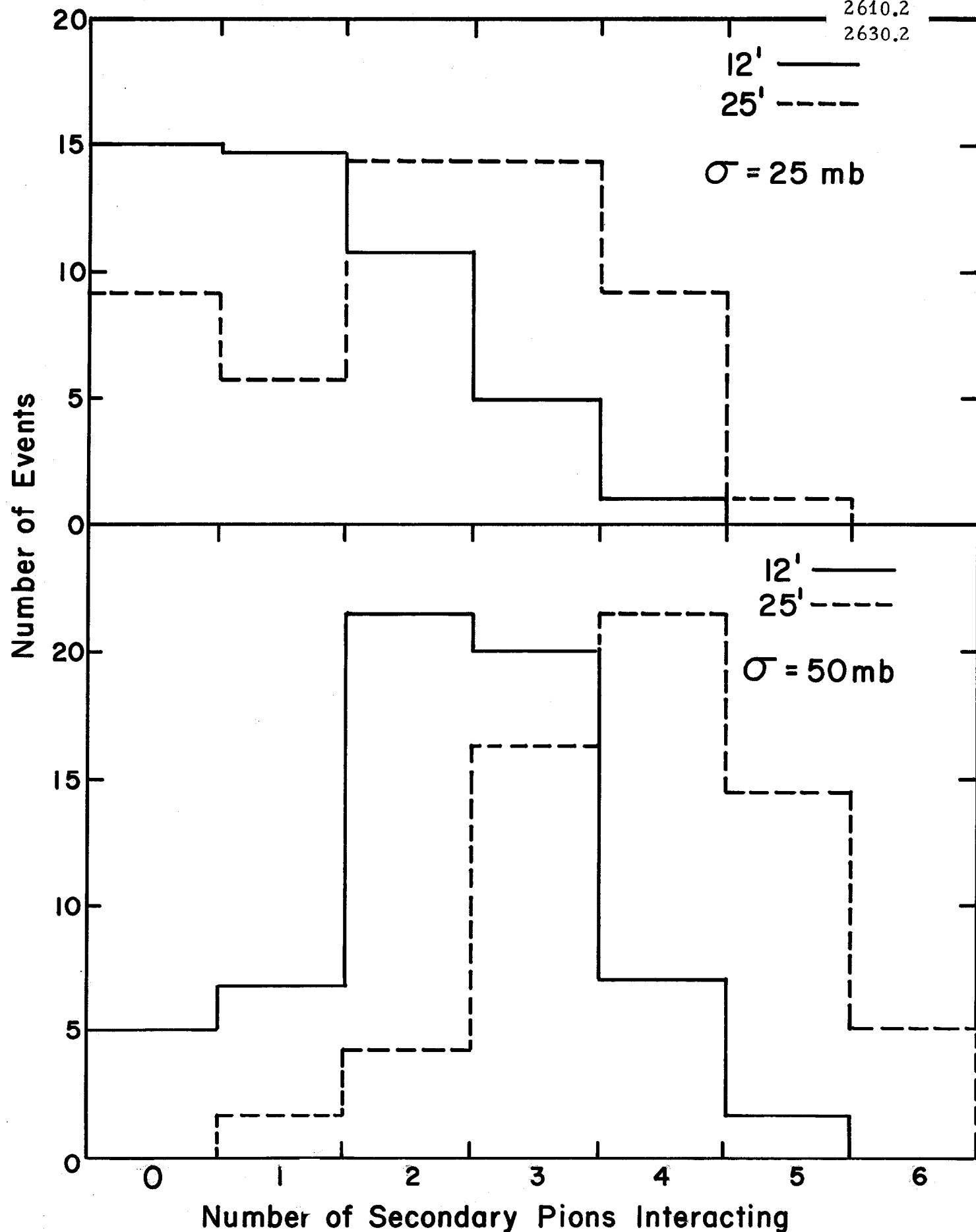


Fig. 20. For a 200-event sample, the number of secondary pions interacting, produced in upstream events in the reaction $\bar{p} + p \rightarrow 3\pi^+ 3\pi^-$. For case b, $\sigma = 60 \text{ mb}$; note the absence of any events in the 25-ft chamber with the secondary pions interacting.